Current Plant Biology 45 (2026) 100579

Contents lists available at ScienceDirect

Current Plant Biology

journal homepage: www.elsevier.com/locate/cpb

Dissecting specialized metabolism in space: A MALDI-MSI atlas of Amaryllidaceae alkaloids in *Hippeastrum papilio* (Ravenna) Van Scheepen

Nuwan Sameera Liyanage [a], Natacha Mérindol [a], Sajjad Sobhanverdi [a], Kenneth Munk Pedersen [b], Christian Janfelt [b], Isabel Desgagné-Penix [a,*]

[a] Department of Biochemistry, Chemistry, Physics, and Forensic Science, Université du Québec à Trois-Rivières, Trois-Rivières, QC, Canada
[b] Toxicology and drug metabolism group, Department of Pharmacy, University of Copenhagen, Universitetsparken 2, Copenhagen DK-2100, Denmark

ARTICLE INFO

Keywords:
Amaryllidaceae alkaloids
Spatial metabolomics
Galanthamine
Haemanthamine
Metabolite transport
Mass spectrometry imaging
Metabolite localization

ABSTRACT

Amaryllidoideae produce specific specialized metabolites called Amaryllidaceae alkaloids (AAs), known for their pharmacological potential. The spatial distribution and biosynthesis within plant tissues, however, remain poorly understood. This study investigates organ- and tissue-specific localization in *Hippeastrum papilio*, from precursors to galanthamine and haemanthamine, using matrix-assisted-laser-desorption/ionization mass-spectrometry-imaging (MALDI-MIS). AAs consistently accumulated in epidermal and vascular tissues; leaves showed uniform distribution across ages and positions, bulbs had higher concentrations in outer-scales and basal-plates, while roots displayed compartmentalized patterns, with galanthamine uniquely abundant in vascular bundles. Haemanthamine and galanthamine were detected in leaf and bulb mucilage, while precursors were scarce. Multivariate analyses revealed that precursors clustered separately from end-products, enriched in middle-scales and apical leaves of bulbs. Nonetheless, biosynthetic intermediates occurred in all tissues, indicating widespread AA biosynthesis. Transcript profiling confirmed differential expression of biosynthetic genes across leaves, bulbs, and roots, consistent with the widespread and multi-organ biosynthesis of AAs revealed by MSI. These findings suggest a coordinated metabolic network in *H. papilio*, challenging existing hypotheses on organ-specific AA biosynthesis and hinting at the transport of end products. This study refines current models of alkaloid biosynthesis and underscores the value of *H. papilio* as a promising resource for sustainable production of therapeutic AAs.

1. Introduction

The Amaryllidaceae (*s.s.*) comprises diverse flowering plants commonly known as amaryllis or daffodils, with notable ecological, ornamental, and pharmacological significance [5]. Belonging to the order Asparagales, this family includes approximately 75 genera with around 900 species, primarily characterized by their bulbous growth forms, linear leaves, and showy, often fragrant flowers [37,38]. Beyond their ornamental appeal, the Amaryllidaceae family holds significant medicinal value. For centuries, traditional medicine systems in various cultures have employed these plants to treat ailments ranging from skin disorders and wounds to more complex conditions such as epilepsy and inflammation [25,42]. Ethnopharmacological practices often rely on a rich array of specialized metabolites, mainly isoquinoline-derived alkaloids with a wide range of pharmacological activities, drawing considerable attention from the scientific community [26,5,42]. More than 700 distinct Amaryllidaceae alkaloids (AAs) have been identified, with notable representatives, including galanthamine, lycorine, and haemanthamine [24]. Galanthamine, has become a therapeutic agent for Alzheimer's disease symptoms due to its acetylcholinesterase inhibitory activity [20,35]. The current supply of these compounds is limited, primarily sourced from the extraction of only a few Amaryllidaceae species, such as *L. aestivum* and *Narcissus pseudonarcissus, Lycoris radiata, and Ungernia victoris* [2,4], highlighting the need to identify more highly productive species and understand their biosynthetic pathways.

Some *Hippeastrum* species, such as *Hippeastrum papilio* have been reported to produce high amounts of galanthamine and haemanthamine, as well as several other AAs (Fig. 1), holding promise for sustainable and efficient extraction relative to other plant sources [2,16,19,

* Corresponding author.
E-mail addresses: Nuwan.Sameera.Liyanage@uqtr.ca (N.S. Liyanage), Natacha.Merindol@uqtr.ca (N. Mérindol), sajjad.sobhanverdi@uqtr.ca (S. Sobhanverdi), kenneth.pedersen@sund.ku.dk (K.M. Pedersen), christian.janfelt@sund.ku.dk (C. Janfelt), Isabel.Desgagne-Penix@uqtr.ca (I. Desgagné-Penix).

https://doi.org/10.1016/j.cpb.2026.100579
Received 14 October 2025; Received in revised form 5 December 2025; Accepted 2 January 2026
Available online 3 January 2026

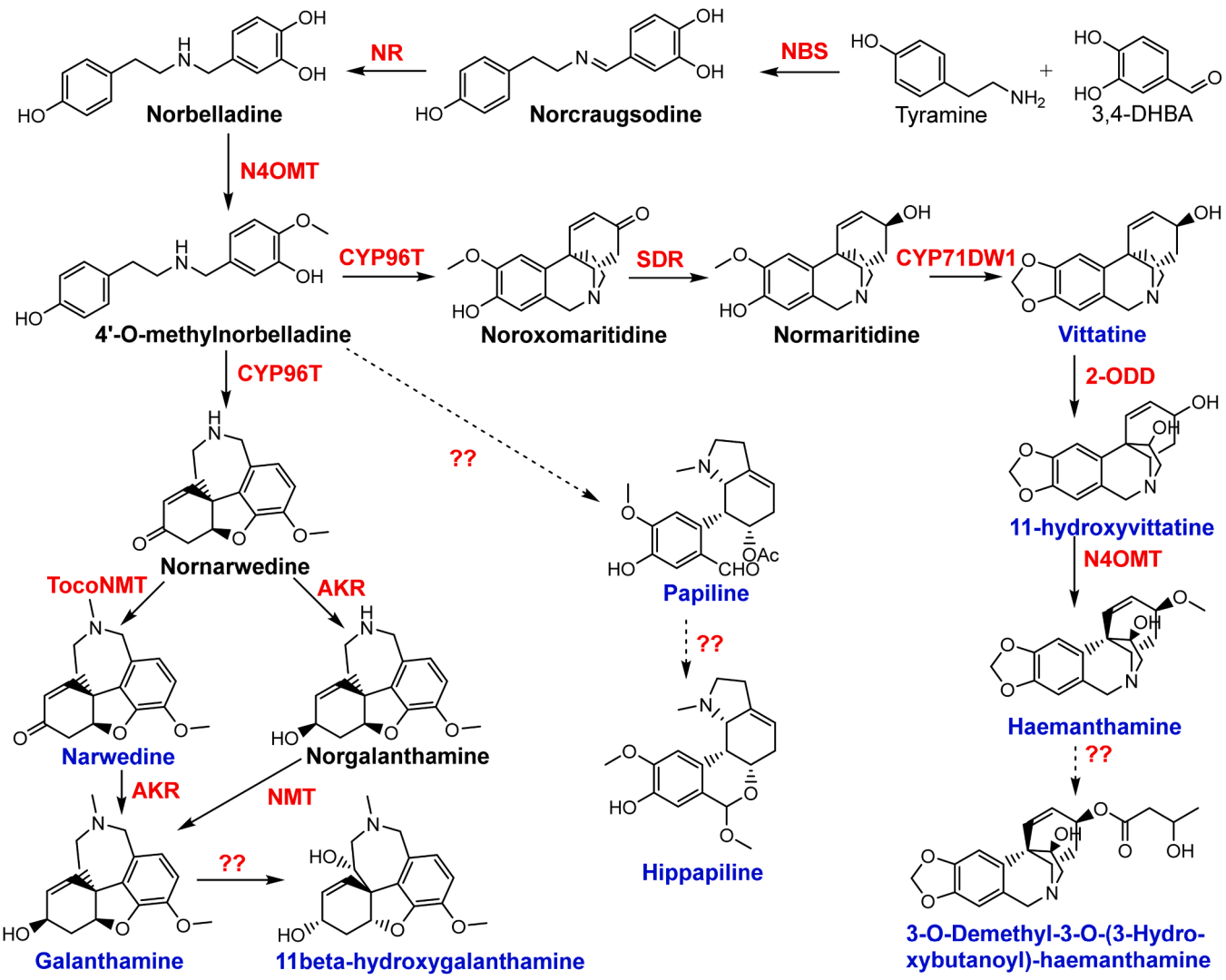

Fig. 1. Biosynthetic pathway representing Amaryllidaceae alkaloids from *Hippeastrum papilio* starting from the initial precursors, tyramine and 3,4-dihydroxybenzaldehyde (3,4-DHBA). The bold letters (black and blue) represent the compounds examined in this study, and the blue letters indicate the alkaloids previously recorded in *H. papilio*. Single arrows represent a single enzymatic reaction, whereas the dotted arrows signify multiple enzymatic steps. Red letters indicate the characterized enzymatic reactions of the pathway. NBS: Norbelladine synthase, NR: Norcraugsodine/noroxomaritidine reductase, N4OMT: Norbelladine 4'-O-methyltransferase, CYP96T: Cytochrome P450 96 T, TocoNMT: Tocopherol N-methyltransferase, AKR: Aldoketoreductase, SDR: Short chain dehydrogenase/reductase, NMT: N-methyltransferase, 2-ODD: 2-oxoglutarate-dependent dioxygenase [19,3,34,39].

49]. *H. papilio*, commonly known as the Butterfly Amaryllis, stands out for its unique floral morphology and the significance of its natural habitats [14]. Originating from the Atlantic forests of southern Brazil, *H. papilio* naturally grows as an epiphyte on tall trees, unlike most geophytic Amaryllidaceae species [9]. Unravelling the precise tissue and organ distribution of specific alkaloids in this species is required to provide the critical knowledge to optimize the species' industrial and pharmaceutical applications. Various techniques have been employed for the *in situ* detection of metabolites in plants, including autofluorescence, staining, labelling, and, more recently, mass spectrometry imaging (MSI) [12,45]. Recent research has begun to explore alkaloid distribution at both histochemical and organ-specific levels of *H. papilio*, shedding light on their biosynthetic pathway using Dragendorff's reagent [19]. Haist et al. demonstrated that alkaloids are present in all plant tissues, with higher concentrations in bulbs (inner part, followed by outer scales) and roots than in leaves. Alkaloids were enriched in phloem sap of leaves, bulbs, roots, leaf parenchyma, and vascular bundles. However, Dragendorff's staining lacks the resolution to identify individual alkaloid components and is prone to false positivity for non-nitrogenous oxygenated compounds [17].

MSI works by ionizing molecules from the surface of a sample and analyzing their mass-to-charge ratios to create molecular maps that represent the spatial localization of specific compounds [15,6]. It has been employed to unravel biosynthetic pathways, allowing researchers to trace the origin, transformation, and final deposition sites of plant metabolites [22,47]. Matrix-assisted laser desorption/ionization (MALDI)-MSI uses a laser to desorb and ionize analytes with an applied chemical matrix, whereas desorption electrospray ionization (DESI)-MSI employs a stream of charged droplets to sample analytes directly from the surface, making it ideal for analyzing delicate plant tissues [22,6]. In Amaryllidaceae, DESI-MSI showed that the leaf bases of *Narcissus* cv. Tête-à-Tête preferentially accumulated vittatine synthesized from radiolabelled 4'-O-methylnorbelladine, whereas mid-leaf accumulated non-radiolabeled lycorine [39]. In *Narcissus tazetta*, MALDI-MSI revealed that galanthamine was mainly concentrated in future leaves (inner bulb), while lycorine and tazettine did not exhibit a discernible distribution pattern within the bulb. No significant differences in distribution were observed among the three alkaloids in the leaf cross-sections [43]. These studies emphasize the diversity of alkaloid repartition among species, organs, tissues, and structural types, and

Table 1
Exact masses and ionized forms of the compounds imaged by MALDI-MSI.

Alkaloid	Molecular formula	Monoisotopic mass (Da)	[M+H]+	[M+K]+	Known isomers
Norcraugsodine	$C_{15}H_{15}NO_3$	257.10518	258.11245	296.06833	n.a.
Norbelladine	$C_{15}H_{17}NO_3$	259.12083	260.12810	298.08398	n.a.
4'-O-Methylnorbelladine	$C_{16}H_{19}NO_3$	273.13648	274.14375	312.09963	Norgalanthamine, Normaritidine
Nornarwedine	$C_{16}H_{17}NO_3$	271.12083	272.12810	310.08398	Noroxomaritidine, Vittatine
Narwedine	$C_{17}H_{19}NO_3$	285.13648	286.14375	324.09963	n.a.
Norgalanthamine	$C_{16}H_{19}NO_3$	273.13648	274.14375	312.09963	4'-O-methylnorbelladine, Normaritidine
Galanthamine	$C_{17}H_{21}NO_3$	287.15213	288.15940	326.11528	n.a.
11β-Hydroxygalanthamine	$C_{17}H_{21}NO_4$	303.14704	304.15431	342.11019	n.a.
Noroxomaritidine	$C_{16}H_{17}NO_3$	271.12083	272.12810	310.08398	Nornarwedine, Vittatine
Normaritidine	$C_{16}H_{19}NO_3$	273.13648	274.14375	312.09963	4'-O-methylnorbelladine, Norgalanthamine
Vittatine	$C_{16}H_{17}NO_3$	271.12083	272.12810	310.08398	Nornarwedine, Noroxomaritidine
11-Hydroxyvittatine	$C_{16}H_{17}NO_4$	287.11574	288.12301	326.07889	n.a.
Haemanthamine	$C_{17}H_{19}NO_4$	301.13139	302.13866	340.09454	n.a.
3-O-Demethyl-3-O-(3-hydroxybutanoyl)-haemanthamine	$C_{20}H_{23}NO_6$	373.15251	374.15978	412.11566	n.a.
Papiline	$C_{19}H_{23}NO_5$	345.15760	346.16487	384.12075	n.a.
Hippapiline	$C_{18}H_{23}NO_4$	317.16269	318.16996	356.12584	n.a.
Di-hexose (Sucrose)	$C_{12}H_{22}O_{11}$	342.11616	343.12344	381.07932	n.a.

n.a.: not applicable

reveal the importance of detailed spatial mapping. They also underscore the need for a comprehensive, multi-organ MSI atlas on high-galanthamine-producing species.

By focusing on the tissue-specific localization of alkaloids in *H. papilio*, this study aims to enhance our understanding of its phytochemistry and potential as a high-value bioresource. We used MALDI-MSI to provide a detailed analysis of the tissue distribution of AAs and their biosynthetic partners in *H. papilio*. A combination of principal component analysis (PCA), *t*-distributed stochastic neighbor embedding (*t*-SNE), Spearman correlation, and hierarchical clustering analyses was employed to isolate the structure- and tissue-specific distribution patterns of *H. papilio* alkaloids, aiming to elucidate their biosynthetic compartmentalization. RT-qPCR was then applied to different organ sections to validate the proposed biosynthetic model. This study addresses two critical questions: a. in which tissues and organs do galanthamine and intermediates predominantly accumulate in *H. papilio*? and b. do other key AAs, such as haemanthamine, exhibit similar spatial arrangements within the plant tissues? This current analysis provides the first multi-organ MALDI-MSI atlas of a high-galanthamine-producing *Hippeastrum* species, offering insights into the tissue-specific biosynthesis and accumulation of AAs, and shedding light on their ecological functions and regulatory mechanisms.

2. Materials and methods

2.1. Plant material

Mature bulbs (4 bulbs in flowering level maturity) of *H. papilio* were purchased from Fluwel V.O.F., Belkmerweg 20 A, 1754 GB Burgerbrug, The Netherlands (https://www.fluwel.com/en-gb/products/amaryllis-papillio). The plants were grown in garden soil mixed with perlite to enhance root aeration, in plastic pots placed on a windowsill for 6 months, with watering as needed. Once the plants had fully entered their vegetative stage, they were uprooted, and the soil was carefully removed, thoroughly washed with tap water, and patted dry. The plants were then sectioned systematically. For the leaves, outer, middle, and inner leaves were sampled, and from each leaf, leaf tip, leaf mid, and the leaf base were separated. From the bulbs, a 2–3 outer scales, middle scales, and inner scales, along with the basal plate were sectioned for the analysis. Roots were separated into three sections: root base, middle, and tip. To minimize ice crystal formation due to the high-water content of the plant, samples were immediately dipped in 5 mM sucrose in phosphate-buffered saline for 30 min after sectioning. Following this, they were washed three times with distilled water to remove excess sucrose from around the tissues. After drying them quickly with tissues, the sections were frozen on a metal sheet over dry ice.

2.2. Sample preparation for MALDI-MSI

Samples were cryo-sectioned using techniques adapted from those developed by Kawamoto and employed for sample embedding by Montini et al. Kawamoto, Kawamoto [29,30,41]. Briefly, an n-heptane and dry ice slurry was prepared in a Dewar jar. A 2.5 × 2.0 cm mold (SECTION-LAB Co. Ltd.) was filled with a 3 % (w/v) carboxymethyl cellulose aqueous gel and partially submerged in the n-heptane dry ice slurry. The samples were inserted into the embedding medium as the edges began to freeze, and the mold was then carefully immersed in n-heptane until the gel solidified completely. Once frozen, the block was removed from the mold and stored at −80°C before being cryo-sectioned. In this case, it was nine leaf cross sections per block, seven cross sections from the bulb tissues per block, and six cross sections of roots per block per biological replicate were taken in the main MSI experiments. A Leica CM3050S cryo-microtome (Leica Microsystems, Wetzlar, Germany) was utilized to create cryo-sections of embedded plant samples at a temperature of −20 °C. The sample was appropriately trimmed using the cryo-microtome before sectioning. Tape-assisted cryo-sectioning at 10–20 μm thickness was performed by using cryo-film (SECTION-LAB Co. Ltd., Hiroshima, Japan). After sectioning, the sections were mounted on regular glass slides with the tissue side upwards using double-sided carbon tape (Electron Microscopy Sciences, Hatfield, PA, USA). The slides with the cryo-sections were stored at −80 °C until the MALDI imaging analysis.

Cryo-sectioned samples were placed in a vacuum desiccator for ten minutes for desiccation. An Olympus BH-2 microscope with reflected light was then used to capture optical images of the plant samples. Next, an iMatrixSpray was used to apply a solution of 2,5-dihydroxybenzoic acid (DHB) (30 mg/mL in 90 % MeOH) as the MALDI matrix [48]. The sprayer settings were established at a height of 80 mm, with a line distance of 1 mm, a speed of 90 mm/s, a density of 3 μL/cm^2, and a total of 15 cycles over a 40 × 40 mm area. Following this, MALDI-MSI data were obtained after the evaluation of crystal formation using compound light microscopy.

2.3. MALDI-MS analysis

A Thermo QExactive Orbitrap mass spectrometer (Thermo Scientific,

Bremen, Germany), equipped with an AP-SMALDI5 ion source (TransMIT GmbH, Giessen, Germany), was utilized for MALDI mass spectrometry imaging (MSI). The instrument was operated with a scan range of *m/z* 100–600 and a mass resolving power of 140,000 at *m/z* 200. Data were collected in positive ion mode (minimum n = 2 per organ). The matrix peak of DHB (*m/z* 273.03937) was used as a lock mass for internal mass calibration, ensuring a mass accuracy of ±1 ppm. For each organ, MSI was performed on two independent biological replicates (n = 2) that met quality criteria for section integrity and matrix crystallization. Pixel size varied depending on the experiment (30 μm or 40 μm for full-organ comparisons; 5–10 μm for high-resolution regions). Pixel size details are reported in each figure legend. Available Amaryllidaceae alkaloid standards were tested in the MALDI-MS prior to the analysis to confirm the detection of the compounds (Supplementary Fig. A1a-A1g).

2.4. Data processing and image generation

The "RAW + UDP to IMZML" program (version 1.6R170; TransMIT, Bremen, Germany) was used to convert the raw data files into imzML files [46]. Mass images were then generated using MSiReader v1.02 [7], with a mass tolerance of 1 ppm. All MSI ion intensities were normalized to total ion current (TIC) before generating images and conducting multivariate analyses to reduce variability across replicates. The color scale was adjusted to enhance the visibility of the compounds of interest. Table 1 provides the masses of the studied compounds in their protonated and deprotonated forms. We included only the AAs that have been previously reported in *H. papilio* and their biosynthetic intermediates, as mentioned in Fig. 1 [2,16,19]. Di-hexose ($[C_{12}H_{22}O_{11} + K]+$, *m/z* 381.07937) was used as a tissue marker to outline the contours. The MS images are representative of both studies and were produced using n = 2 biological replicates. All the data generated in this study was uploaded to the Metaspace metabolite annotation data platform for mass spectrometry imaging data (https://metaspace2020.org/) (see data availability), and annotated with KEGG-V1, ChEBI-2018–01, HMDB-v4, and NPA-2019–08 databases [44].

2.5. Mucilage analysis

While sampling the tissues of *H. papilio* leaves and bulbs, the secreted mucilage was collected from three positions on the leaves (leaf tip, mid, and base) and the bulb into Eppendorf tubes, and kept on ice. Mucilage samples were collected from three biological replicates and processed independently. To precipitate proteins, a 1:1 ratio of methanol was added to the collected mucilage (50 μL mucilage + 50 μL methanol), followed by vortexing and centrifugation at 10,000 rpm for 15 min. A 10 μL supernatant was diluted in 90 μL deionized water with papaverine at 1 ppm as the internal standard before analysis by LC-MS.

2.6. LC-MS analysis

A high-performance liquid chromatography (HPLC) system (Agilent 1100, USA) combined with a tandem quadrupole mass spectrometer (Waters Micromass Quattro Micro, USA), equipped with an electrospray ionization (ESI) source, was utilized for the alkaloid analysis. Chromatographic separation was performed using a Phenomenex Kinetex biphenyl column (75 × 2.1 mm, 2.6 μm, 100 Å pore size) maintained at a constant temperature of 30°C. A volume of five microliters from each sample was injected onto the column, which maintained a flow rate of 0.3 mL/min. The mobile phase consisted of solvent A (Milli-Q water with 0.1 % formic acid) and solvent B (methanol with 0.1 % formic acid). The elution gradient was as follows: from 0 to 5 min, isocratic at 10 % B; from 5 to 7 min, a linear increase to 25 % B; from 7 to 10 min, a ramp to 98 % B; from 10 to 15 min, held at 98 % B; from 15 to 16 min, a return to 10 % B; and reconditioning from 16 to 25 min.

The mass spectrometer was operated under the following source conditions: a cone voltage of 30 V, a source temperature of 120°C, a desolvation temperature of 300°C, and a desolvation gas flow rate of 500 L/h. Analysis was conducted in multiple reaction monitoring (MRM) mode, with three ion transitions monitored for each compound to ensure specificity and sensitivity. Detailed information on all transitions and compound-specific parameters can be available in Supplementary Table A1. Relative quantitative analysis was conducted using calibration curves generated from standard solutions of the target alkaloids, which were processed with internal standards (compound/papaverine ratio). Data acquisition and processing were managed using MassLynx software (Waters, version details if applicable). The results were visualized and statistically analyzed using GraphPad Prism v10.

2.7. Dimension reduction and multivariate clustering analyses

Organ-level normalized abundance data and binary fine-tissue × organ-zone localization profiles were compiled into structured matrices for multivariate analysis. Metabolite frequency values were standardized using z-score to ensure comparable scales across variables. For each variable x, z was calculated as $z = (x - \mu)/\sigma$, where μ and σ are the mean and standard deviation across all tissues, respectively. Principal component analysis (PCA) was applied to the organ-level abundance matrix, to capture global variance in metabolite distribution patterns. A hybrid matrix was then constructed by integrating the binary fine-tissue localization data with normalized organ-level abundance values. This matrix was likewise z-score standardized and subjected to PCA to assess spatial localization and tissue-level accumulation trends jointly. *t*-Distributed Stochastic Neighbor Embedding (*t*-SNE) was performed on the hybrid matrix using the following parameters: perplexity = 5, learning rate = 200, number of iterations = 3000, and random seed = 42. This allowed visualization of metabolite relationships in a two-dimensional space while preserving the local neighborhood structure of the high-dimensional input. Pairwise Spearman's rank correlation coefficients were calculated from the hybrid matrix, and a hierarchical clustering heatmap was generated to validate metabolite groupings based on spatial and quantitative similarity. The PCA and t-SNE axes are unitless and optimized, respectively, for variance explanation and neighborhood preservation. Assistance from generative AI tools (ChatGPT, OpenAI GPT-4, 2024 release) was used to develop the initial Python scripts. All code was critically reviewed, iteratively adjusted, and executed locally on the authors' laboratory computers. The final analyses and figure generation were performed entirely offline, using these customized scripts in interaction with the AI to improve reproducibility, visualization clarity, and parameter selection.

Statistical differences in individual feature distributions between precursor metabolites and other alkaloid groups were assessed using a two-tailed Mann-Whitney *U* test. Hierarchical clustering was applied to the z-score standardized hybrid matrix using Ward's linkage and Euclidean distance. Although the original matrix includes binary tissue localization features, standardization produced a continuous distribution of feature values, allowing the application of Ward's method [28,10]. This approach yielded a dendrogram consistent with known biosynthetic relationships among alkaloids.

2.8. Total RNA extraction and qRT-PCR

Total RNA was extracted using a modified cetyltrimethylammonium bromide (CTAB) protocol based on Meisel et al. [40] with three biological replicates. Approximately 200 mg of finely ground tissue (using liquid nitrogen) was homogenized in 2 mL of CTAB lysis buffer supplemented with 10 % (v/v) β-mercaptoethanol and 50 μL of spermidine trihydrochloride. The homogenate was incubated at 65 °C for 10 min in a water bath to ensure efficient cell lysis. Phase separation was then carried out by adding 1 mL of chloroform:isoamyl alcohol (24:1, v/v), followed by vigorous vortexing for 30 s and centrifugation at 13,000 rpm for 15 min. This step was repeated once to remove proteins.

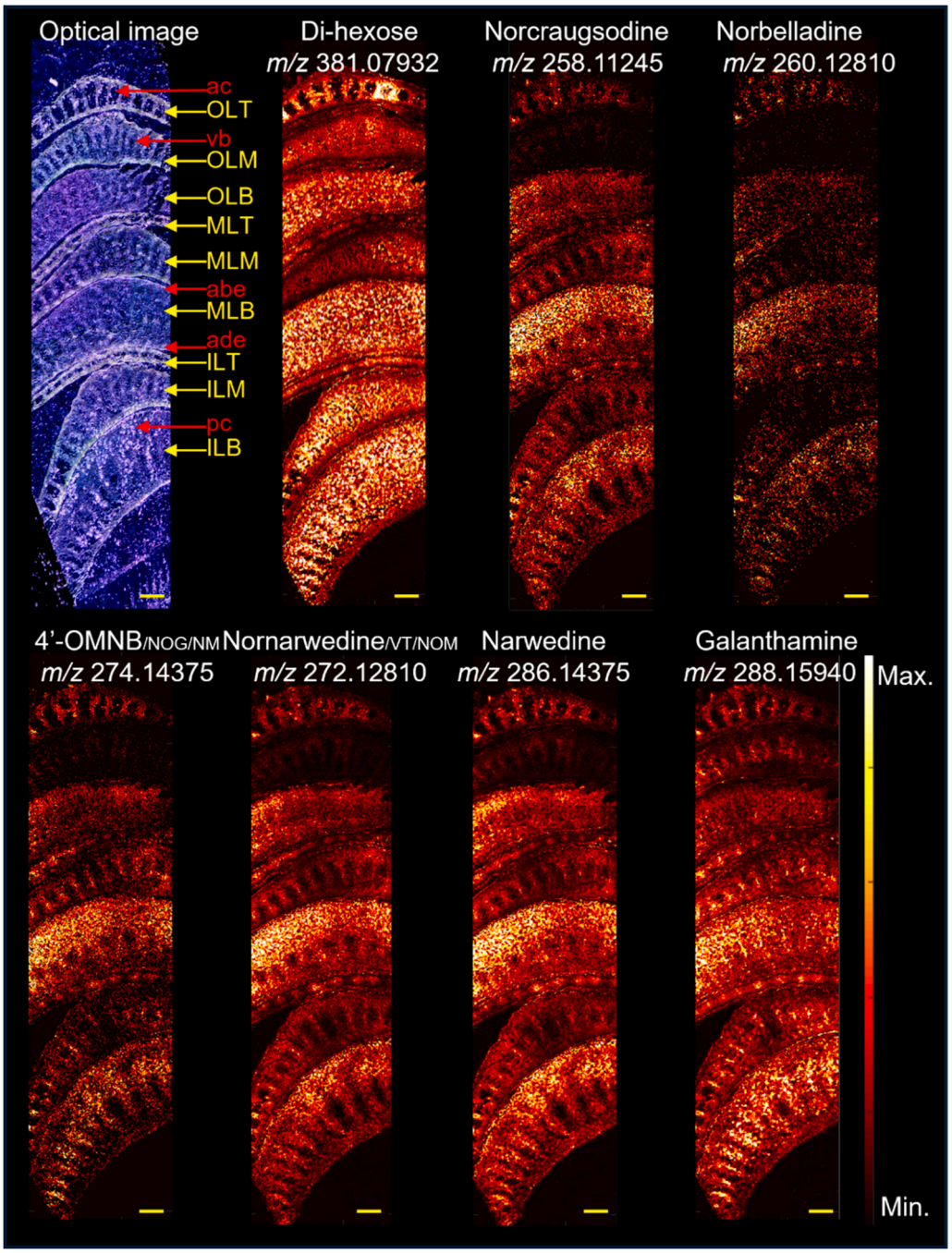

Fig. 2a. MALDI-MSI of *Hippeastrum papilio* leaf cross sections. From top to bottom, yellow arrows indicate the position of the leaf sections: outermost leaf (OLT = tip, OLM = mid, OLB = base), middle leaf (MLT = tip, MLM = mid, MLB = base), and innermost leaf (ILT = tip, ILM = mid, ILB = base). Red arrows indicate tissue types: ac = aerenchyma, vb = vascular bundles, abe = abaxial (lower) epidermis, ade = adaxial (upper) epidermis, and pc = parenchyma. Compound abbreviations: 4′OMNB = 4′-O-methylnorbelladine, NOG = norgalanthamine, NM = normaritidine, VT = vittatine, and NOM = noroxomaritidine. Pixel size: 40 μm, Biological replicates: n = 2 independent plants (one representative shown), Ion mode: [M+H]+ ions, TIC-normalized, Compound identification: accurate mass (±1 ppm) and confirmed with available standards, Scale bar: 1 mm. Imaging was performed on two plants; the representative MSI obtained from one plant is shown.

The resulting aqueous phase was transferred to a new tube and mixed with an equal volume of 10 M lithium chloride, followed by overnight incubation at −20 °C to precipitate RNA. The RNA was pelleted by centrifugation at 15,000 rpm for 45 min, washed with 80 % cold ethanol, and air-dried at room temperature. The dried pellet was resuspended in 50 μL of RNase-free water and treated with the TURBO DNA-free™ Kit (Invitrogen) to remove genomic DNA contamination. After inactivating DNase, final RNA purification was performed using the Monarch® RNA Cleanup Kit according to the manufacturer's instructions. The relative expression levels of genes involved in AA biosynthesis, including *TYDC1*, *TYDC2*, *NBS*, *NR*, *OMT*, *CYP96T1*, and *NMT* (Supplementary Table A2) were quantified using the One Step Luna® Universal qRT-PCR Kit (New England Biolabs). *Actin* was used as the internal reference gene for normalization, as the *histone3* candidate was not stably expressed. Each qRT-PCR reaction was performed with gene-specific primers and 100 ng of total RNA in a final reaction volume 10 μl. Amplification and detection were carried out on the CFX Connect™ Real-Time PCR Detection System (Bio-Rad). The $2^{-\Delta Ct}$ method was used to calculate relative expression of each transcript relative to actin in each tissue.

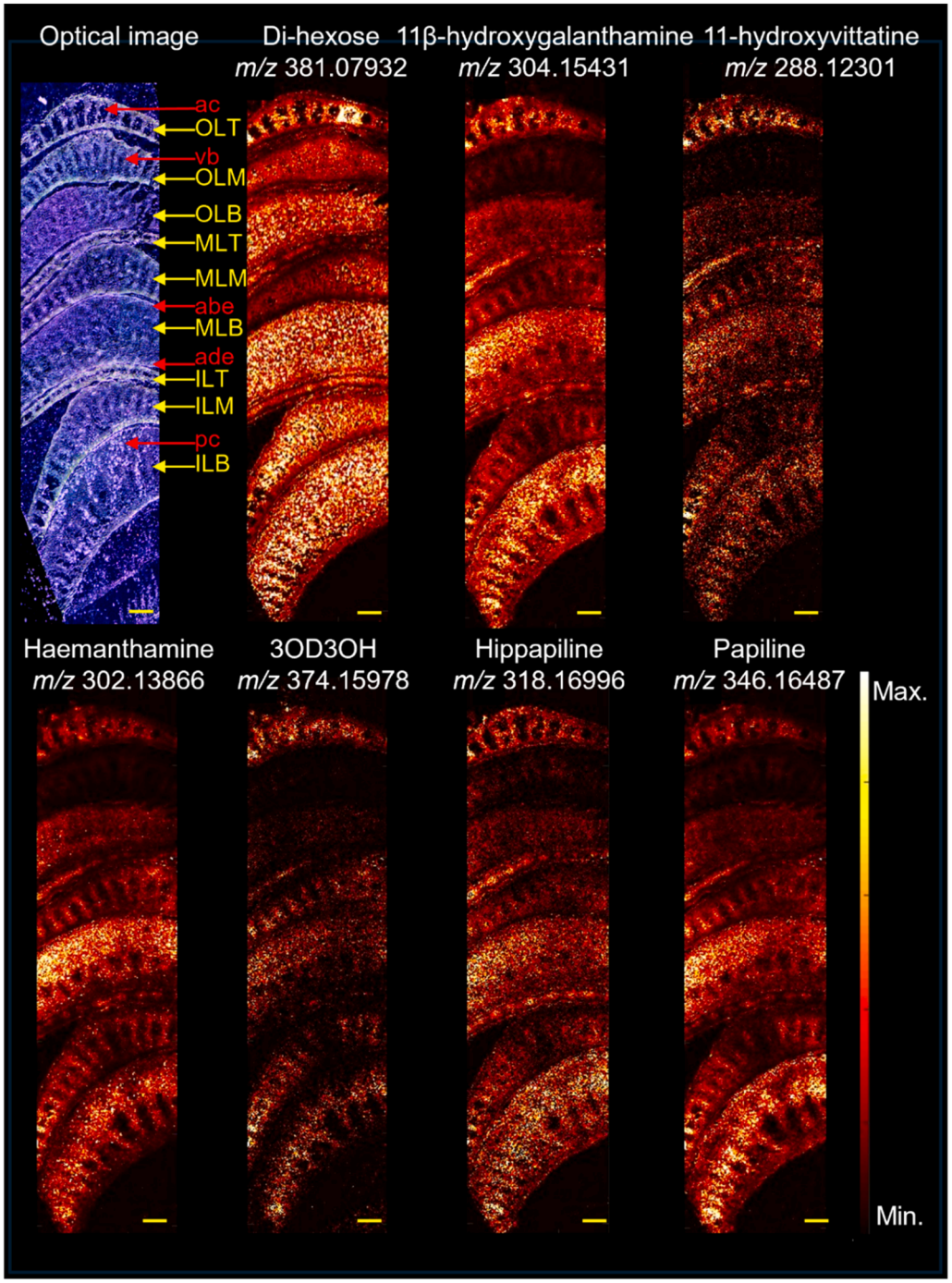

Fig. 2b. MALDI-MSI of *Hippeastrum papilio* leaf cross sections. From top to bottom, yellow arrows indicate the position of the leaf sections: outermost leaf (OLT = tip, OLM = mid, OLB = base), middle leaf (MLT = tip, MLM = mid, MLB = base), and innermost leaf (ILT = tip, ILM = mid, ILB = base). Red arrows indicate tissue types: ac = aerenchyma, vb = vascular bundles, abe = abaxial (lower) epidermis, ade = adaxial (upper) epidermis, and pc = parenchyma. Compound abbreviation: 3OD3OH = 3-O-demethyl-3-O-(3-hydroxybutanoyl)-haemanthamine. Pixel size: 40 μm, Biological replicates: n = 2 independent plants (one representative shown), Ion mode: [M+H]+ ions, TIC-normalized, Compound identification: accurate mass (±1 ppm) and confirmed with available standards, Scale bar: 1 mm.

3. Results

The spatial distribution of AAs was analyzed in sections of the leaves, bulb scales, and roots of *H. papilio*, using MALDI-MSI. Images of di-hexose were included in each MSI experiment to outline the morphology and contours of the analyzed tissues and serve as internal references for spatial orientation. Compound detection was based on accurate mass measurements and comparison to authenticated standards. Although MALDI-MSI is inherently semi-quantitative, and ion intensities do not directly reflect absolute compound abundance due to potential variability in ionization efficiency, the structural similarity of the alkaloids provided a reasonable basis for cautious comparison of their ion intensities. This approach allowed us to gain insight into the relative distribution and accumulation trends of major versus minor alkaloids across tissues.

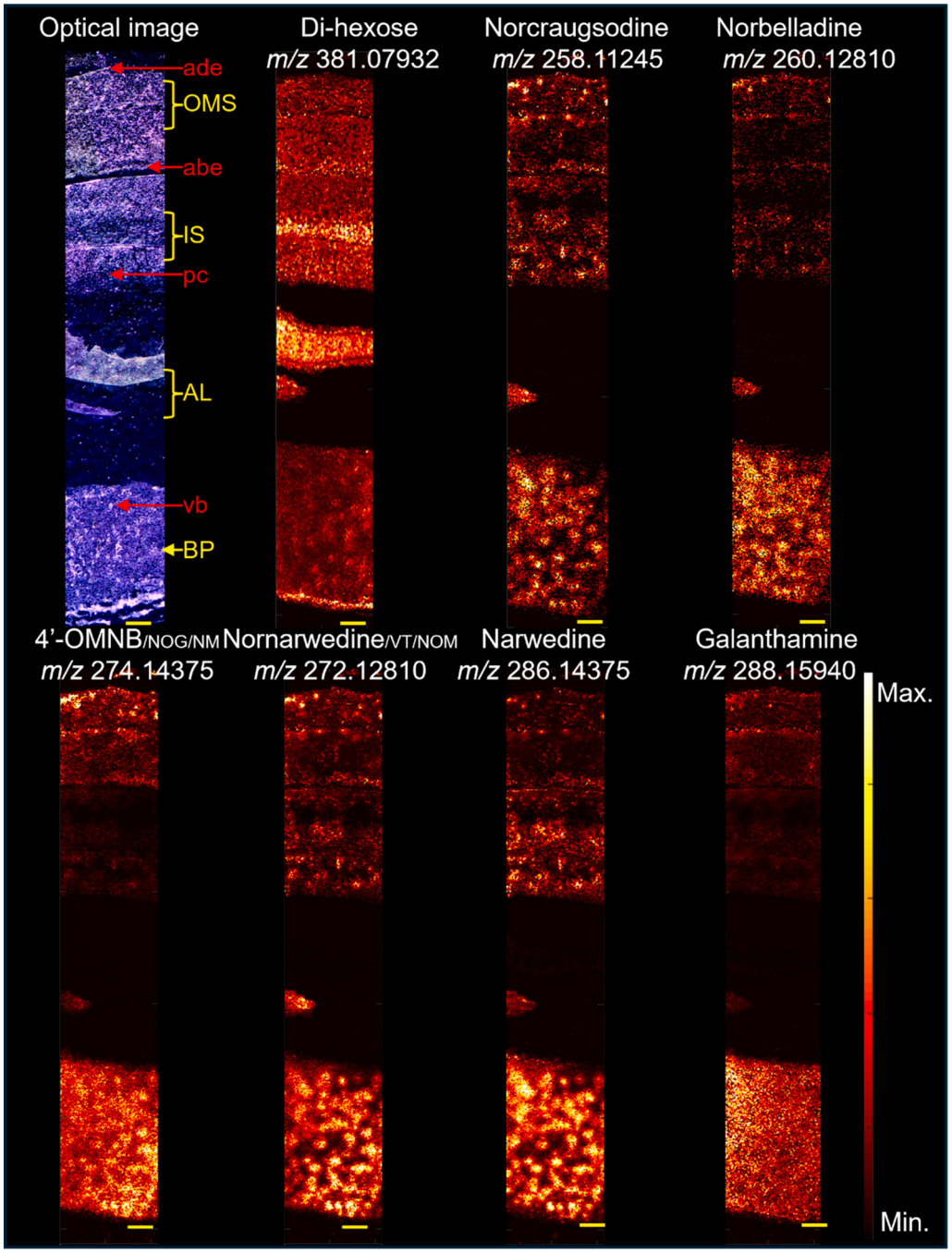

Fig. 3a. MALDI-MSI of *Hippeastrum papilio* bulb cross sections. In each panel, from top to bottom, yellow arrows indicate the position of the tissue sections: OMS = outermost scales (two sections), IS = inner scales, AL = apical leaves (two sections), and BP = basal plate. Red arrows denote tissue types: ade = adaxial (outer) epidermis, abe = abaxial (inner) epidermis, pc = parenchyma cells, and vb = vascular bundles. Compound abbreviations: 4′OMNB = 4′-O-methylnorbelladine, NOG = norgalanthamine, NM = normaritidine, VT = vittatine, and NOM = noroxomaritidine. Pixel size: 30 μm, Biological replicates: n = 2 independent plants (one representative shown), Ion mode: [M+H]+ ions, TIC-normalized, Compound identification: accurate mass (±1 ppm) and confirmed with available standards, Scale bar: 1 mm.

3.1. *Amaryllidaceae alkaloids in H. papilio leaf tissues*

H. papilio innermost, middle, and outermost leaves were segmented into three anatomical regions, i.e., the leaf base, mid-leaf, and leaf tip, resulting in a total of nine cross sections per plant (Fig. 2a). The sections were embedded together in a 3 % (w/v) carboxymethyl cellulose gel as a single block and scanned to generate a comprehensive image, allowing comparison of signal intensities across the individual samples (Figs. 2a, 2b; Supplementary Table A1).

The leaves of *H. papilio* exhibited typical monocotyledonous anatomical features. The MALDI-MSI analysis focused initially on the spatial distribution of 12 alkaloids spanning the AA biosynthetic pathway (Fig. 1), including early precursors such as norcraugsodine (*m/z* 258.1125) and norbelladine (*m/z* 260.1281) (Fig. 2a; top panels), major products like galanthamine (*m/z* 288.1594), and haemanthamine (*m/z* 302.1386), and several derivatives such as 11β-hydroxygalanthamine (*m/z* 304.1543) and 3-O-demethyl-3-O-(3-hydroxybutanoyl)-haemanthamine (*m/z* 374.1597) (Figs. 2a, 2b; Supplementary Table

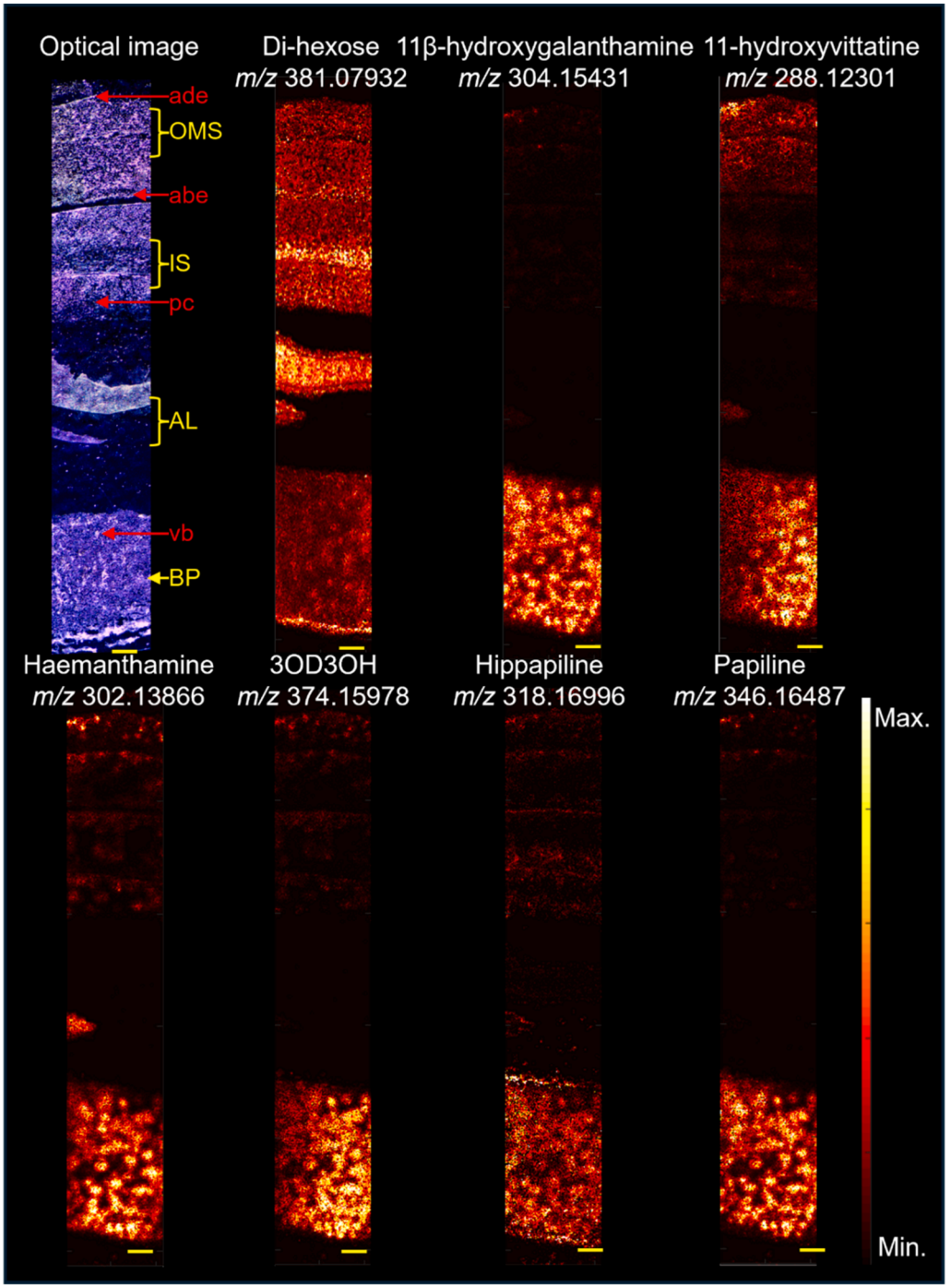

Fig. 3b. MALDI-MSI of *Hippeastrum papilio* bulb cross sections. In each panel, from top to bottom, yellow arrows indicate the position of the tissue sections: OMS = outermost scales (two sections), IS = inner scales, AL = apical leaves (two sections), and BP = basal plate. Red arrows denote tissue types: ade = adaxial (outer) epidermis, abe = abaxial (inner) epidermis, pc = parenchyma cells, and vb = vascular bundles. Compound abbreviation: 3OD3OH = 3-O-demethyl-3-O-(3-hydroxybutanoyl)-haemanthamine. Pixel size: Pixel size: 30 μm, Biological replicates: n = 2 independent plants (one representative shown), Ion mode: [M+H]+ ions, TIC-normalized, Compound identification: accurate mass (±1 ppm) and confirmed with available standards, Scale bar: 1 mm.

A1). Imaging was performed at a pixel size of 40 μm, with selected tissues imaged at higher resolutions of 10 μm and 5 μm for finer structural detail (Supplementary Fig. A2 and in Metaspace https://metaspace2020.org/).

Among the detected signals, galanthamine and haemanthamine exhibited the highest ion intensities, which was consistent with their known accumulation as major AAs in *H. papilio*. Intermediate compounds such as norcraugsodine, norbelladine, and 4′-O-methylnorbelladine (including isomers norgalanthamine and normaritidine), as well as minor alkaloids like hippapiline and 3-O-demethyl-3-O-(3-hydroxybutanoyl)-haemanthamine, were detected at comparatively lower ion intensities. While intensities do not translate linearly into compound abundances, they suggest that biosynthetic intermediates and minor alkaloids are present throughout leaf tissues at substantially lower concentrations than major alkaloids. Norcraugsodine, norbelladine, 4'-O-methylnorbelladine/norgalanthamine/normaritidine, narwedine/vittatine/ noroxomaritidine, 11-hydroxyvittatine, haemanthamine, and 3-O-demethyl-3-O-(3-hydroxybutanoyl)-

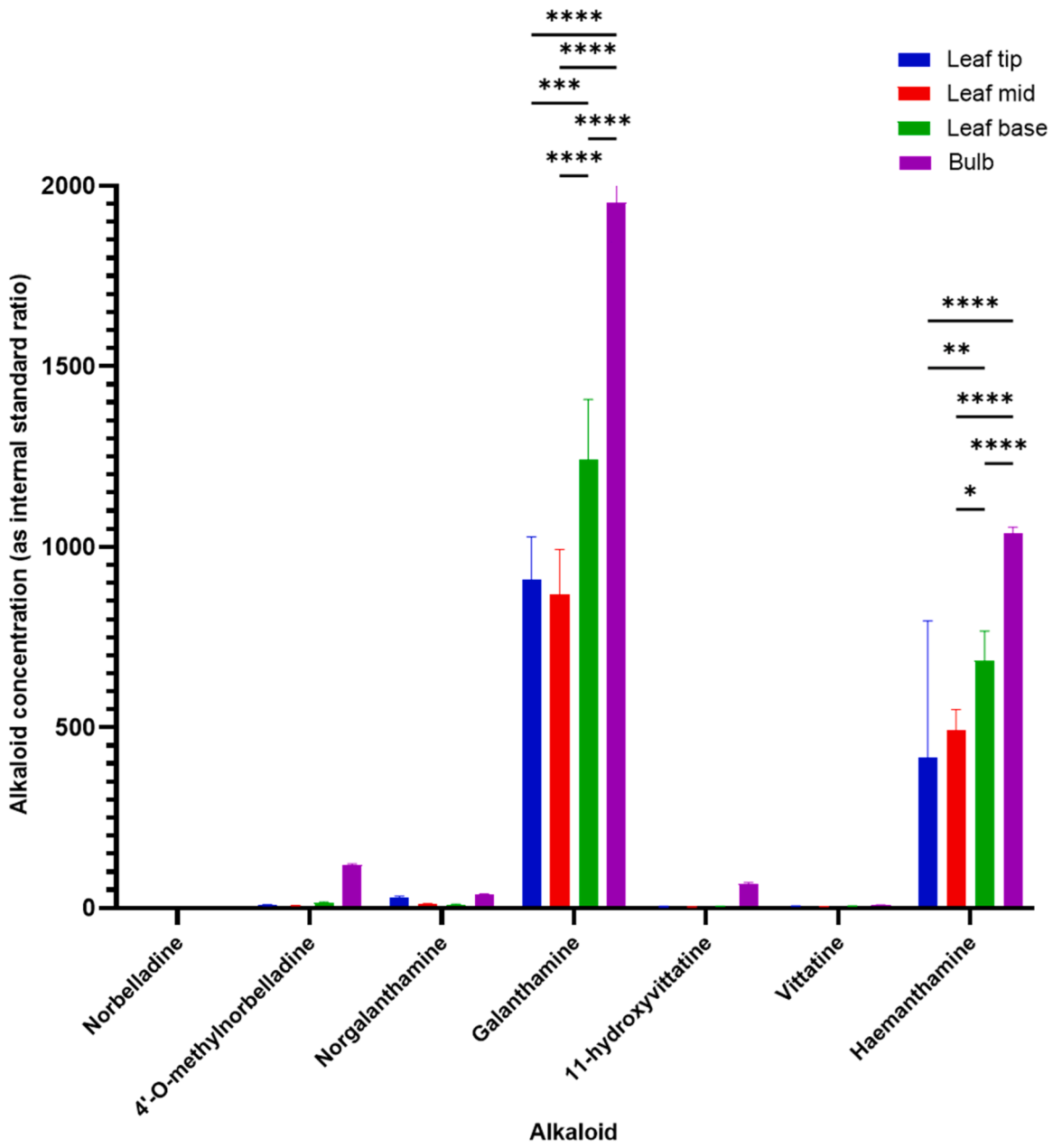

Fig. 4. Alkaloid comparison of the mucilage of *Hippeastrum papilio*. Alkaloid contents were measured by LC-MS/MS and normalized using the papaverine internal standard. All the values are shown as means ± standard deviation of three independent biological replicates. *P*-values presented as Dunnett's multiple comparisons test of one-way ANOVA. **** = $p < 0.0001$, *** = $p < 0.001$, ** = $p < 0.01$, * = $p < 0.1$. Non-significant interactions are not presented in the graph. Mucilage was collected from three independent biological replicates.

haemanthamine were not detected in the midsection of the outermost leaves (Figure 2).

Almost all metabolites were detected in epidermal tissues, vascular bundles, and mesophylls (parenchyma), with higher abundances observed in the epidermal and vascular regions, particularly in the lower epidermal areas of the leaf bases (Supplementary Figure A2, Figure 2). In contrast, AAs were absent in the aerenchyma, consisting primarily of air spaces within the leaf tissues. Norbelladine and 3-O-demethyl-3-O-(3-hydroxybutanoyl)-haemanthamine were not detected in the outer epidermis layer, possibly corresponding to the cuticle, although this was not confirmed histologically. 4'-O-Methylnorbelladine/norgalanthamine/normaritidine, papilline-type, and galanthamine-type consistently accumulated in vascular bundles of most cross 3-O-Demethyl-3-O-(3-hydroxybutanoyl)-haemanthamine was not detected in most epidermal tissues. Overall, galanthamine displayed the broadest and most uniform distribution across both tissues and leaf regions, highlighting its dominance among the alkaloids detected in *H. papilio* leaf tissues.

Thus, the spatial distribution patterns of each alkaloid were remarkably consistent across different leaf ages (outermost to innermost leaves) and positions (base, mid, and tip), though some were absent from specific zones, such as the midsection of the outermost leaves. Together, these patterns indicate that leaf tissues are active sites of biosynthetic activity. The detection of multiple biosynthetic intermediates alongside end-products in the same tissues suggests that several steps of AA biosynthesis occur locally within leaves.

3.2. *Amaryllidaceae alkaloids in H. papilio bulb tissues*

Alkaloid localization was further investigated on two outer scales,

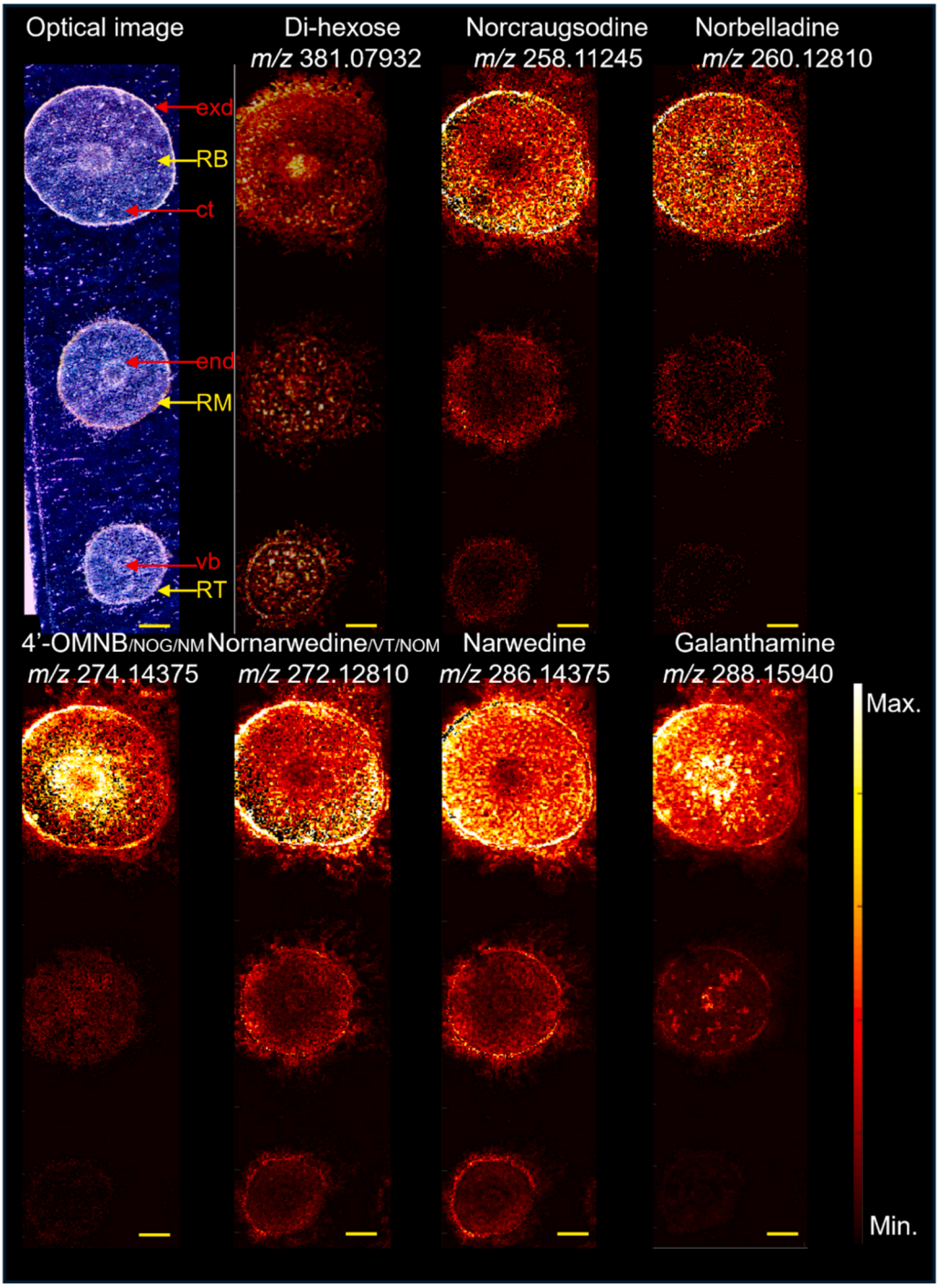

Fig. 5a. MALDI-MSI of *Hippeastrum papilio* root cross sections. In each panel, from top to bottom, yellow arrows indicate the position of the tissue sections: RB = root base, RM = root middle, and RT = root tip. Red arrows indicate tissue types: exd = exodermis, ct = cortex, end = endodermis, and vb = vascular bundles. Compound abbreviations: 4′OMNB = 4′-O-methylnorbelladine, NOG = norgalanthamine, NM = normaritidine, VT = vittatine, and NOM = noroxomaritidine. Pixel size: 40 μm, Biological replicates: n = 2 independent plants (one representative shown), Ion mode: [M+H]+ ions, TIC-normalized, Compound identification: accurate mass (±1 ppm) and confirmed with available standards, Scale bar: 1 mm.

two middle scales, two apex leaves (leaf primordia) of *H. papilio* bulbs, and a portion of the basal plate, all embedded together in a single imaging block. All 12 alkaloids previously identified in leaf tissues were detected in the bulb (Figs. 3a and 3b, Supplementary Table A1). Alkaloid signals were predominantly concentrated in the basal plate. Norcraugsodine, norbelladine, narwedine, and nornarwedine/vittatine/noroxomaritidine were consistently dispersed across both outer and inner bulb scales (Supplementary Table A1). In contrast, 4'-O-methylnorbelladine/norgalanthamine/normaritidine, galanthamine, 11-hydroxyvittatine, haemanthamine, and hippapiline were more abundant in the outer scales. Intermediates norcraugsodine, norbelladine, nornarwedine, narwedine, as well as haemanthamine, and papilline were detected in one of the apical leaves, while others were not.

Norbelladine, 11β-hydroxygalanthamine, 11-hydroxyvittatine, haemanthamine, and 3-O-demethyl-3-O-(3-hydroxybutanoyl)-haemanthamine were not detected in the outer epidermis layer (possibly the cuticle) of bulb scales. Metabolites were more abundant in the basal plates' vascular bundles, except galanthamine, which was evenly

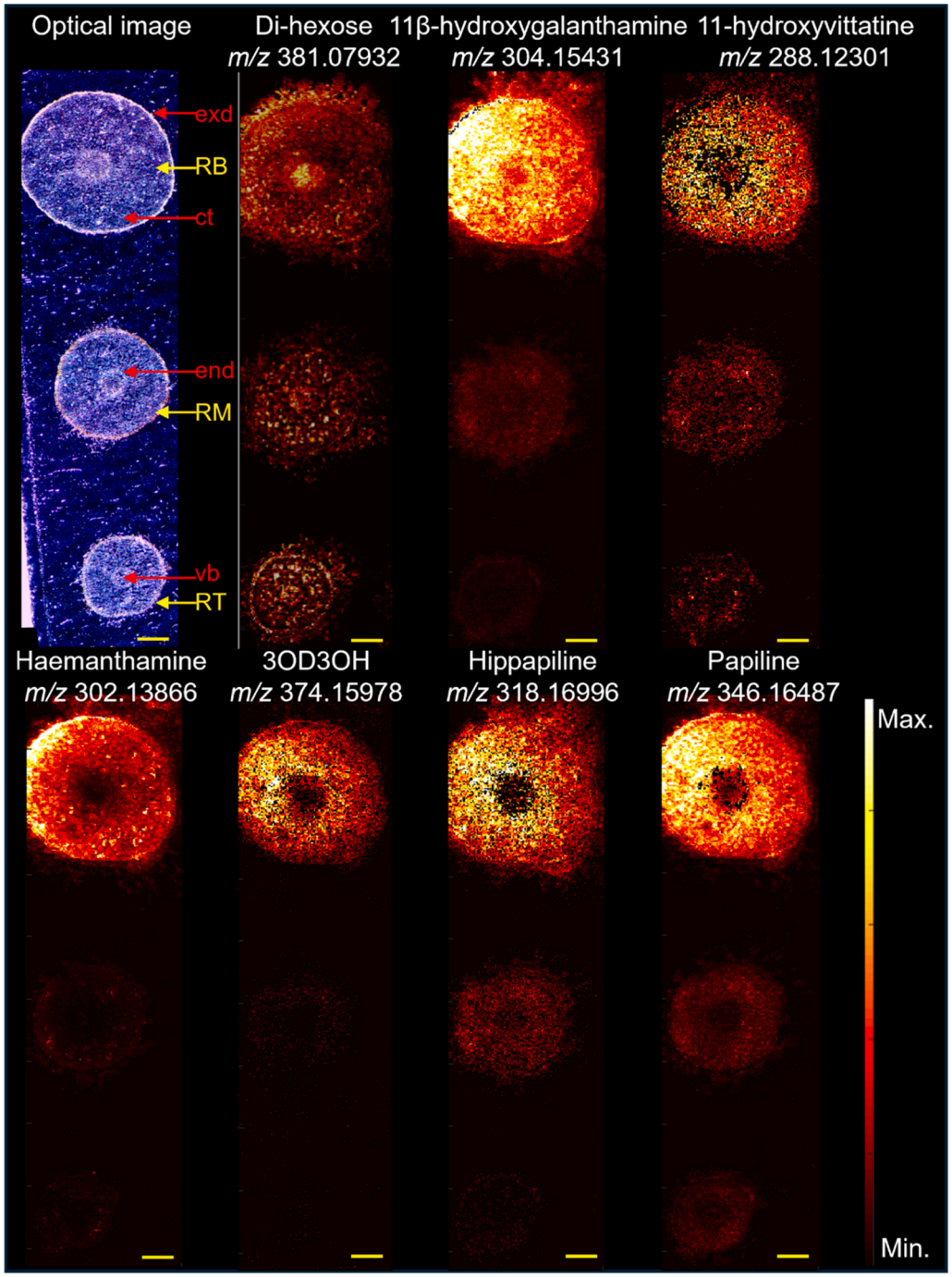

Fig. 5b. MALDI-MS images a cross sections of *Hippeastrum papilio* root tissues. In each panel, from top to bottom, yellow arrows indicate the position of the tissue sections: RB = root base, RM = root middle, and RT = root tip. Red arrows indicate tissue types: exd = exodermis, ct = cortex, end = endodermis, and vb = vascular bundles. Compound abbreviation: 3OD3OH = 3-O-demethyl-3-O-(3-hydroxybutanoyl)-haemanthamine. Pixel size: 40 μm, Biological replicates: n = 2 independent plants (one representative shown), Ion mode: [M+H]+ ions, TIC-normalized, Compound identification: accurate mass (±1 ppm) and confirmed with available standards, Scale bar: 1 mm.

distributed throughout the basal plate tissues.

Galanthamine, haemanthamine, 11β-hydroxygalanthamine, narwedine, and papiline were the most abundant alkaloids in *H. papilio* bulb tissues. These were followed by 4'-O-methylnorbelladine/norgalanthamine/normaritidine, nornarwedine/ noroxomaritidine/vittatine, and 11-hydroxyvittatine. Biosynthetic intermediates such as norcraugsodine and norbelladine, as well as minor alkaloids like hippapiline and 3-O-demethyl-3-O-(3-hydroxybutanoyl)-haemanthamine, were detected at relatively lower ion intensities. These findings suggest that while biosynthetic intermediates and minor alkaloids are present throughout the bulb tissues, their concentrations are lower than those of the major alkaloids.

In addition to internal organ analysis, we collected mucilage from the leaf and bulb of *H. papilio* and measured the concentrations of alkaloids and precursors (Fig. 4). Only alkaloids for which standards were available were included. Interestingly, intermediate compounds, such as norbelladine, 4'-O-methylnorbelladine, and norgalanthamine, were poorly detected in this waxy substance, except for a significant detection

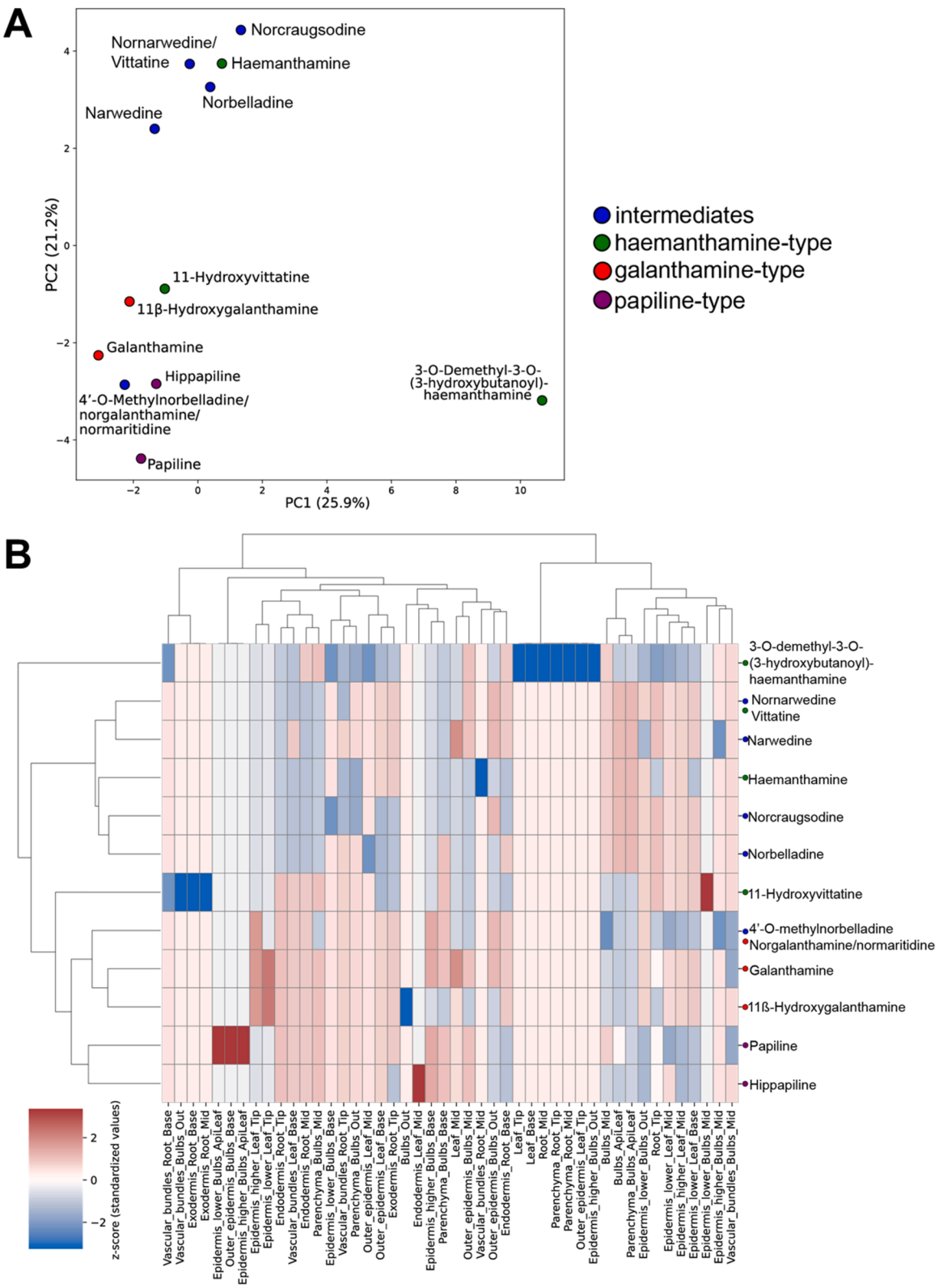

Fig. 6. Integrated analysis of alkaloid distribution in *Hippeastrum papilio* tissues. **A.** Principal component analysis of Supplementary Table A1, integrating organ-level detection frequency and fine-tissue × organ-zone localization data. The matrix was standardized before dimensionality reduction. Metabolites are color-coded by chemical group. **B.** Hierarchical clustering of alkaloids based on their spatial distribution across organs and fine tissue zones. The hybrid matrix integrates organ-level detection frequencies and binary fine-tissue × organ-zone localization data, both standardized using z-score transformations. Clustering was performed using Ward's linkage and Euclidean distance, and the resulting heatmap displays the relative spatial profiles of each alkaloid (rows) across all anatomical features (columns). Row colors denote chemical classes: blue = precursor/intermediate compounds, red = galanthamine-type, green = crinine-type, purple = papiline-type. The dendrogram reflects groupings based on overall similarity in tissue-level detection, with a cophenetic correlation coefficient r = 0.77, indicating a match between clustering topology and original data structure.

of 4'-O-methylnorbelladine in the mucilage coming from the bulb (119.713 ± 3.235 relative concentration as internal standard responsive ratio). However, galanthamine (733.26–1952.634 relative concentration as internal standard responsive ratio) and haemanthamine (417.205–1036.464 relative concentration as internal standard responsive ratio) were detected in high amounts in the mucilage of the two organs. Interestingly 4'-O-methylnorbelladine (8.11 times higher than leaf base, $p = 0.0113$), 11'-hydroxyvittatine (14.64 times than leaf base, $p < 0.0001$), galanthamine (1.57 times than leaf base, $p < 0.0001$), and haemanthamine (1.51 times than leaf base, $p < 0.0001$) were significantly higher in the mucilage extracted from the bulb compared to leaf cross-sections (Fig. 4). These findings confirm that end-products accumulate in both leaves and bulbs and are present in greater amounts than their precursors.

Overall, the distribution patterns of alkaloids in bulb tissues differed markedly from those observed in leaf tissues. Variations in spatial localization were observed both between tissue layers and among different anatomical regions within the bulb. At the tissue level, alkaloids were predominantly detected in vascular bundles, epidermal tissues, and parenchyma. The spatial patterns observed in the bulb suggest that *H. papilio* bulbs are not passive reservoirs but active hubs of AA biosynthesis. The pronounced enrichment of AAs in mucilage and vascular tissues further supports a role for bulbs in both synthesis and redistribution.

3.3. Amaryllidaceae alkaloids in H. papilio root tissues

To analyze the AA arrangement in the root tissues of *H. papilio*, single images containing two sections from the beginning, two from the middle, and two from the root tip were included (Figs. 5a, 5b; Supplementary Figure A3, Supplementary Table A1). Alkaloid concentrations were higher at the root base and decreased toward the root tips. At the tissue level, distinct distribution patterns emerged. Almost all tested metabolites were detected in the exodermis, cortex, and vascular bundle regions, with varying intensities (Figs. 5a and 5b). For instance, norcraugsodine, norbelladine, nornarwedine/vittatine/noroxomaritidine, and haemanthamine were abundant in the exodermis and the cortex region adjacent to the exodermis (Supplementary Table A1). In contrast, 4'-O-methylnorbelladine/norgalanthamine/normaritidine showed higher abundance in the exodermis and cortex regions closer to the vascular bundle. Galanthamine was predominantly localized in the exodermis and vascular bundles. Hippapiline and 3-O-demethyl-3-O-(3-hydroxybutanoyl)-haemanthamine were more concentrated in the cortex, while papiline and 11β-hydroxygalanthamine were more abundant in the exodermis and cortex. Thus, the spatial distribution of alkaloids varied significantly across regions, tissue types, and positions along the root, and was more compartmentalized than in leaves and bulbs. AAs were predominantly restricted to the cortex and exodermis of the root base, with narwedine and papiline dominating the chemical landscape. The lower relative abundance of early intermediates suggests that the root may play a more limited or specialized role in alkaloid metabolism.

3.4. Spatial distribution and accumulation clustering of alkaloids in H. papilio

To better understand patterns of localization, spatial distribution of alkaloids, and potential tissue-specific functions in *H. papilio*, we performed a series of multivariate analyses. A hybrid matrix was constructed that combined fine-tissue localization (presence/absence) with detection frequency across organ cross-sections (from Supplementary Table A1). This enabled dimensionality reduction and spatial clustering of alkaloid distribution patterns. A PCA using only normalized detection frequencies across leaf, bulb, and root cross-sectional zones (tip, mid, and base) (Supplementary Figure A4) first grouped metabolites based on their organ-level distribution patterns. Precursor and intermediate compounds, including norcraugsodine, norbelladine, nornarwedine, and narwedine, clustered together, reflecting similar organ cross-section-level distribution. Haemanthamine was positioned close to these precursors. Most other alkaloids appeared more dispersed, indicating greater variability in their spatial profiles (Supplementary Figure A4). 4′-O-methylnorbelladine (co-detected with norgalanthamine and normaritidine) clustered in proximity to galanthamine and 11β-hydroxygalanthamine, suggesting overlapping organ-level accumulation. Conversely, 3-O-demethyl-3-O-(3-hydroxybutanoyl)-haemanthamine was positioned further from the other metabolites, reflecting a more divergent detection profile and possible tissue-specific specialization. A second PCA was performed using a hybrid matrix built from Supplementary Table A1 that combined fine-tissue × organ-zone presence/absence data with organ-level detection frequency values (Fig. 6A). This integrated analysis confirmed the clear separation between precursor/intermediate metabolites (norcraugsodine, narwedine, norbelladine, nornarwedine) and more specialized derivatives, including papiline-type and galanthamine-type alkaloids. 3-O-demethyl-3-O-(3-hydroxybutanoyl)-haemanthamine remained isolated from other compounds, consistent with a distinct tissue localization profile, while 4'-O-methylnorbelladine/norgalanthamine/normaritidine position stayed close to galanthamine. Differences in tissue-level distributions, particularly in the apical bulb leaf and the root tip and mid sections, contributed significantly to the separation between precursor metabolites and galanthamine-type compounds (Mann-Whitney *U* test, $p < 0.05$).

To verify local similarities among metabolites based on their tissue-level distribution, *t*-SNE was applied to the hybrid dataset (Supplementary Figure A4B). The nonlinear dimensionality reduction confirmed the distinct clustering of intermediate compounds (e.g., norbelladine, norcraugsodine, narwedine) from galanthamine-type and papiline-type alkaloids. These clusters further highlighted differences between compounds detected in the apical leaves of the bulb and those enriched in leaf tips and root tissues, reinforcing the notion of tissue-specific specialization along the biosynthetic pathway. A pairwise Spearman correlation analysis was performed on the hybrid matrix to assess similarities in metabolite distribution patterns quantitatively (Supplementary Figure A4C). Positive correlations ($\rho > 0.76$) were observed among intermediate compounds, consistent with their tight clustering in both PCA and *t*-SNE projections. Notably, narwedine and nornarwedine exhibited the highest correlation ($\rho = 0.89$), while galanthamine and 11β-hydroxygalanthamine also showed substantial similarity in their spatial profiles ($\rho = 0.85$). Interestingly, across all multivariate analyses, haemanthamine consistently clustered more closely with intermediate precursors. To further explore alkaloid relationships based on tissue localization patterns, we applied hierarchical clustering using Ward's method to the hybrid matrix (Fig. 6B). This analysis grouped the twelve alkaloids into four main clusters. To assess the reliability of the hierarchical clustering structure, we computed the cophenetic correlation coefficient between the original distance matrix and the dendrogram derived from Ward's method. The resulting coefficient $r = 0.77$ indicated concordance between the dendrogram topology and the underlying data structure, supporting the robustness of the observed alkaloid groupings. The first cluster included the majority of precursor and intermediate compounds, i.e., norcraugsodine, norbelladine, nornarwedine (vittatine/noroxomaritidine), and narwedine, as well as haemanthamine. These compounds were predominantly detected in the apical bulb leaf and the mid-section of the root, with limited presence in the vascular zones. The second cluster comprised 4'-O-methylnorbelladine/norgalanthamine/normaritidine, galanthamine, 11ß-hydroxygalanthamine, and the papiline-type alkaloids (papiline and hippapiline), which were more frequently detected in vascular bundles, leaf base, and root tip tissues, including the endodermis and epidermis. A third cluster contained only 11-hydroxyvittatine, detected in both the cortex and vascular regions of the root and bulb, suggesting a partially overlapping but distinct localization. The fourth cluster grouped 3-O-demethyl-3-O-(3-hydroxybutanoyl)-haemanthamine,

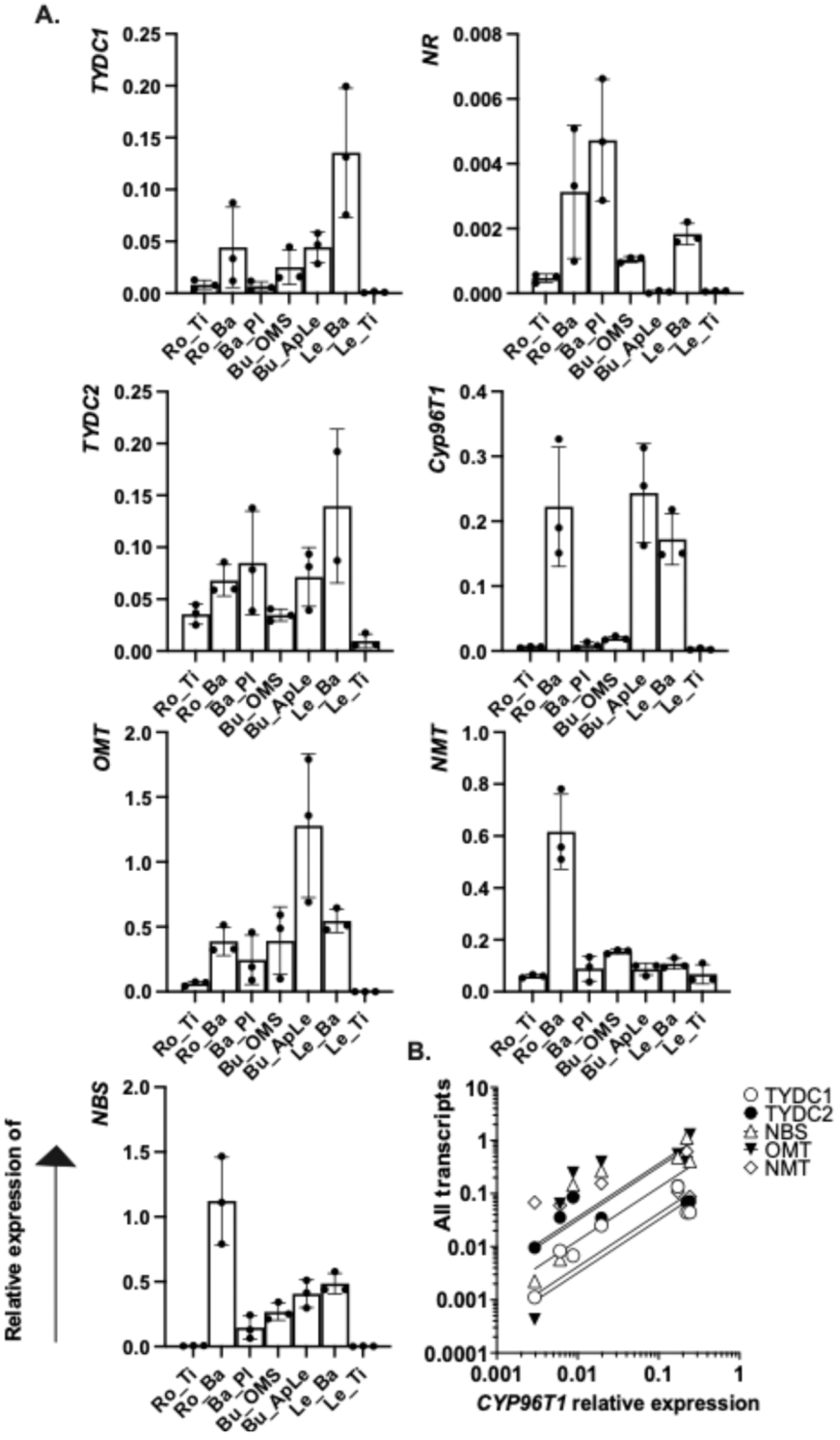

Fig. 7. Amaryllidaceae alkaloid biosynthetic gene candidates' expression levels via RT-qPCR across organ sections. **A.** relative expression of transcripts, tyrosine decarboxylase1 (*TYDC1*), tyrosine decarboxylase2 (*TYDC2*), *O*-methyltransferase (*OMT*), norbelladine synthase (*NBS*), norcraugsodine reductase (*NR*), cytochrome p45096T1 (*CYP96T1*), *N*-methyltransferase (*NMT)* were normalized on the level of actin expression. Ro_Ti= root tip, Ro_Ba = Root base, Ba_Pl = Basal plate, Bu_OMS = Bulb outer middle scale, Bu_ApLe = Bulb apical leaf, Le_Ba = leaf base, Le_Ti= Leaf tip. **B.** Association between levels of expression of CYP96T1 and other transcripts (Pearson correlation). NR expression is not displayed because not significantly associated. RT-qPCR was performed on three independent biological replicates.

which showed a unique pattern, with detection restricted to the bulb parenchyma and mid-root cortex, but absent from most other tissue zones. These groupings were also consistent with the spatial separation patterns observed in the PCA and *t*-SNE analyses.

3.5. Biosynthetic gene candidates' expression across organ sections

To test whether biosynthesis at the transcription levels matched the spatial partitions inferred from MSI, i.e., whether early *vs* late-step gene expression segregates across organs and whether young apical leaf tissue

constitutes a biosynthetic hotspot, we quantified transcripts for seven AA pathway candidates across root, bulb, and leaf sections, normalizing to *actin* and analyzing by the $2^{-\Delta Ct}$ method. We profiled candidates of two entry-point decarboxylases (*TYDC1/2*) [23], the first committed condensation enzyme (*NBS*) and the putative reductase (*NR*) [32], the *O*-methyltransferase acting on norbelladine or precursors (*OMT*), the phenol-coupling P450 (*CYP96T1*) [31], and an *N*-methyltransferase (*NMT*) implicated in galanthamine biosynthesis [39]. Sections assayed were root tip (Ro_Ti), root base (Ro_Ba), basal plate (Ba_Pl), bulb outer middle scale (Bu_OMS), bulb apical leaf (Bu_ApLe), leaf base (Le_Ba), and leaf tip (Le_Ti) to understand the contrast of the same organ related to the position (Fig. 7A). Both *TYDC1* and *TYDC2* peaked at the leaf base (relative expression of *TYDC1* = 0.135 ± 0.062, *TYDC2* = 0.140 ± 0.074), and were lowest at the leaf tip, yielding large dynamic ranges (*TYDC1* ≈ 121-fold; *TYDC2* ≈ 15-fold). *NBS* was strongly enriched at the root base (1.122 ± 0.338), minimal at the leaf tip (0.0023 ± 0.001; ~500-fold range). *NR* transcripts were overall low, with a slight maximum at the basal plate (0.0047 ± 0.001) > root base (0.0031 ± 0.002) and near-baseline in bulb apical leaves (0.000045 ± 0.000043) and the leaf tip (0.000068 ± 0.000012). *OMT* showed a striking expression in bulb apical leaves (1.279 ± 0.553), followed by leaf base (0.545 ± 0.089) and bulb outer middle scales (0.393 ± 0.26). Expression in the leaf tip was near-zero (0.00043 ± 0.001), yielding the most extensive dynamic range (~3,006-fold). Phenol-coupling P450 (*CYP96T1*) mirrored *OMT* with a bulb apical leaves maximum (0.243 ± 0.076) and elevated expression at root base (0.222 ± 0.092) and leaf base (0.172 ± 0.039); while the leaf tip contained the lowest amounts (0.0029 ± 0.001; ~83-fold range). *NMT* was broadly expressed but highest at the root base (0.616 ± 0.145) > bulb outer middle scales (0.155 ± 0.007) ≈ leaf base (0.108 ± 0.02) ≈ basal plate (0.089 ± 0.048) ≈ bulb apical leaves (0.087 ± 0.023); root tip was lowest (0.060 ± 0.006; ~10-fold range).

There was a significant positive correlation of expression between *CYP96T1* and *NBS* (r = 0.810, $p = 0.0074$), *OMT* (r = 0.801, $p = 0.0084$), and *TYDC1* (r = 0.644, $p = 0.0424$); a possible correlation with *TYDC2* (r = 0.603, $p = 0.0567$) and *NMT* (r = 0.533, $p = 0.087$); although not significant (Fig. 7B). *CYP96T1* expression was not correlated with *NR* (r = 0.084, $p = 0.422$). The strongest correlation observed was between *NBS* and NMT (r = 0.907, $p = 0.0009$), consistent with their shared root-base enrichment. The transcript maps supported a division of steps across organs: early/branch-setting and coupling steps (*TYDCs*, *OMT*, *CYP96T1*) were enriched in young apical leaf and leaf base, whereas early condensation and late *N*-methylation capacity (*NBS*, *NMT*) were prominent in basal/root tissues. This distribution was consistent with the MSI-derived separation between zones enriched in precursors/intermediates versus those concentrating downstream alkaloids and specialized cell layers, and it highlighted the apical bulb leaf as a transcriptional hotspot for key mid-pathway steps in *H. papilio* (Fig. 7; MSI multivariate summary in Fig. 6)

3.6. Additional compound annotations with metaspace

In addition to using the comprehensive literature review on alkaloids reported in *H. papilio* as database, we utilized the MSI metabolite annotation platform Metaspace [44] to analyze the data obtained from our non-targeted MSI experiments. Even if the identification in Metaspace is based solely on accurate mass analysis (leaving the possibility open for the presence of several isomeric compounds instead of or in addition to the tentatively identified compound), it revealed the putative presence of multiple classes of compounds (Supplementary Table A3), such as colchicine derivatives (deacetylcolchicine, N-acetoacetyl-deacetylcolchicine, trimethylcolchicinic acid/ N-deacetylcolchiceine, demecolchine/androcymbine/isoandrocymbine) (Supplementary Fig. A5E-H), flavonoids (kaempferol-3-O-rutinoside/ kaempferol 3-O-rhamnoside-7-O-glucoside, luteolin/kaempferol, quercetin 3-O-glucoside, quercetin/8-hydroxykaempferol/6-hydroxykaempferol/8-hydroxyluteolin, 4′-methoxyflavanone), amides (N-*p*-trans-coumaroyltyramine, N-trans-caffeoyltyramine), lignans (1-acetoxypinoresinol, deoxypodophyllotoxin), pigments (pheophorbide a, adonixanthin/ dinoxanthin/ didinoxanthin, echinenone, 4-ketomyxol), and a fungicide (flumetover) (Supplementary Fig. A6, Supplementary Table A3)

Metaspace annotations also indicated the potential presence of AAs not yet reported in *H. papilio*. These included phenanthridine-type alkaloids such as crinasiadine and trisphaeridine, β-carboline alkaloids like trichotamine, and a variety of AA, including assoanine, oxoassoanine, albomaculine, ungeremine, hippeastrine, crinan/gamma-lycorane, O-methyllycorenine, belladine, amaryllisine/lycorenine, and papyramine (Fig. 8, Supplementary Table A3, Supplementary Fig, A5). Additionally, metabolites associated with the alkaloid degradation pathway, such as galanthamine beta-D-glucuronide and O-demethyl-galanthamine beta-D-glucuronide, were identified. These findings highlight the chemical diversity of *H. papilio*.

4. Discussion

Previous models of AA biosynthesis in *Narcissus* species proposed that early intermediates were synthesized primarily in basal leaf regions and then transported to other tissues, where end products accumulate. Studies using radiolabeled precursors in *Narcissus cv.* Tête-à-Tête showed preferential incorporation of 4′-O-methylnorbelladine into vittatine at leaf bases, whereas mid-leaf regions accumulated lycorine [39]. Likewise, MSI investigations in *Narcissus tazetta* reported that galanthamine was enriched in the inner leaf bases, whereas lycorine and tazettine showed less distinct spatial patterns [43]. These studies, however, did not detect intermediates in all organs. Here, we provide a detailed spatial analysis of AAs across leaves, bulbs, and roots of *Hippeastrum papilio*, combining MALDI-MSI, LC-MS, RT-qPCR, and multivariate clustering. We first focused on the repartition of well-known alkaloids end products (such as galanthamine, haemanthamine) and intermediates (such as norbelladine, norcraugsodine) in cross-sections of leaves, bulbs, and roots.

4.1. Leaf tissues

Previous studies have suggested that AAs are biosynthesized in young leaf tissues in *Narcissus cv.* Tête-à-Tête [39]. Consistently, all AAs were detected in the innermost part of the leaf. In contrast, intermediates like norcraugsosine, norbelladine, 4'-O-methylnorbelladine (norgalanthamine, or normaritidine), nornarwedine (vittatine/noroxomaritidine) were detected in some but not all outermost sections of the leaf. Yet, the detection of these intermediates in the base and tip leaf sections suggests that alkaloid biosynthesis may be spatially widespread, not confined to specific regions in *H. papilio*. Their detection at low ion intensities could indicate transient accumulation in the tissues, consistent with their role as precursors for the synthesis of more complex alkaloids [33]. The distribution of galanthamine, papiline, and hippapiline across different leaf ages and positions suggests that they may play a generalized role in leaf physiology and serve analogous functions, such as protecting photosynthetic tissues, maintaining structural integrity, and defending against pathogens and herbivores, rather than being specific to certain developmental stages or regions. This observation is consistent with the findings of Nakagawa et al. [43], who reported no significant differences in the distribution patterns of galanthamine, lycorine, and tazettine in *N. tazetta* leaf tissues [43]. In *Narcissus cv.* Tête-à-Tête alkaloids were localized near vascular tissues of leaves, a finding that resonates with the results presented here [39]. The abundance of alkaloids in epidermal and vascular tissues, particularly in the lower epidermal regions of leaf bases, underscores their potential

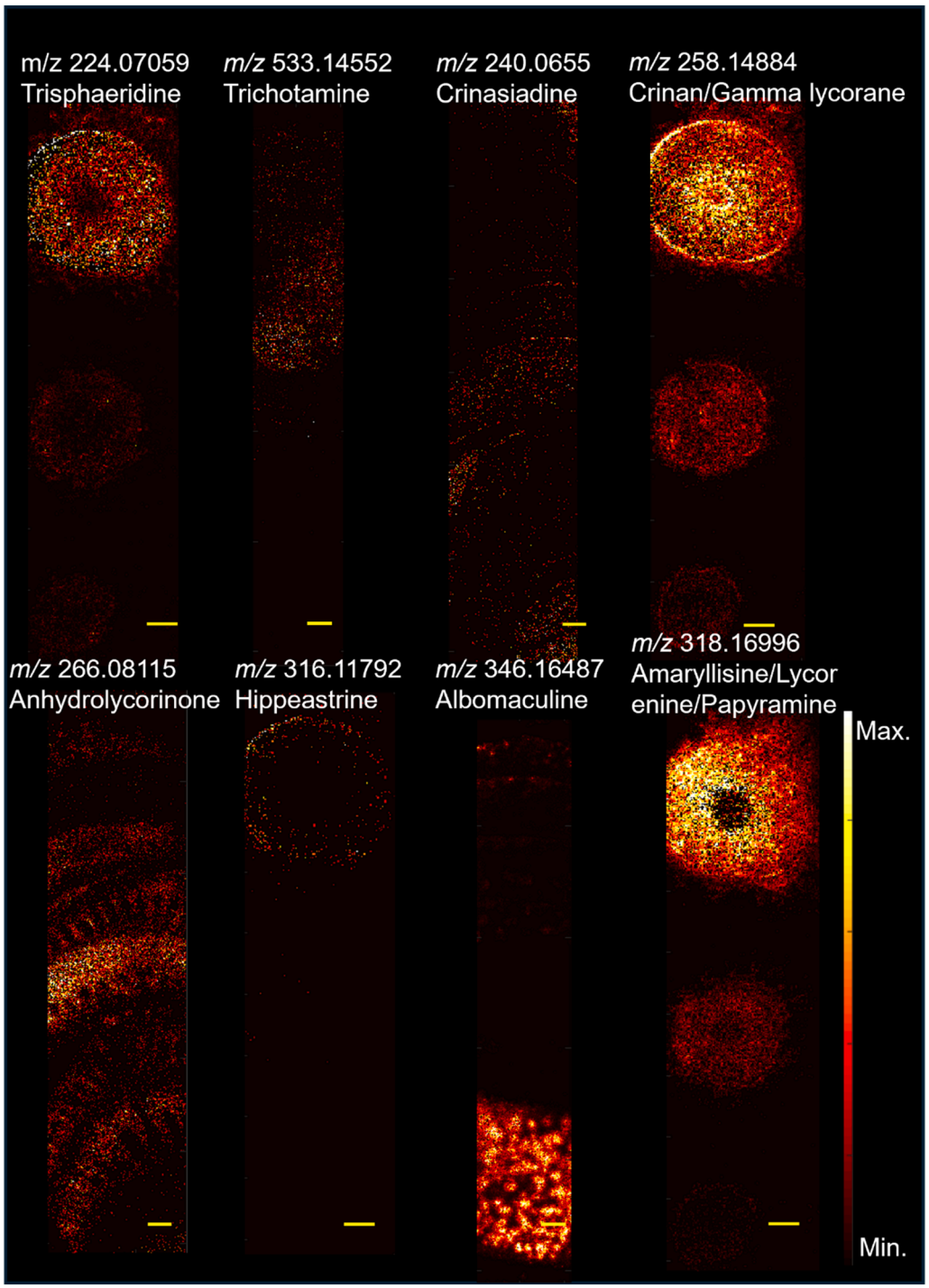

Fig. 8. MALDI-MSI of multiple METASPACE-annotated compounds in cross sections of *Hippeastrum papilio* tissues. Panels A, D, F, and H show root sections (pixel size: 40 μm); panels B and G show bulb sections (pixel size: 30 μm); and panels C and E show leaf sections (pixel size: 40 μm). Biological replicates: n = 2 independent plants (one representative shown), Ion mode: [M+H]+ ions, TIC-normalized, Compound identification: accurate mass (±1 ppm) and confirmed with available standards, Scale bar: 1 mm.

role in defence mechanisms [50]. Epidermal tissues are the first living cells of a plant body that separate the plant from the environment; hence, the presence of alkaloids in these regions may deter herbivory and microbial infections [11]. Similarly, the localization of alkaloids in vascular bundles suggests their involvement in systemic defence and possibly their transport [18]. The absence of alkaloids in the aerenchyma supports the idea that these compounds are strategically localized in tissues with higher metabolic activity and defence requirements. This finding aligns with the histochemical localization study by Haist et al. [19], which detected alkaloids in the cuticle, vascular bundles, intracellular spaces, nucleus, and vacuoles of *H. papilio* leaf tissues [19].

4.2. Bulb tissues

LC-MS analysis revealed that AAs accumulated more in the mucilage of bulbs than in leaves in *H. papilio*. There was also a greater variation in AA repartition across the bulbs' cross-sections. AA accumulated intensely in the basal plates, followed by the outermost bulb scales and

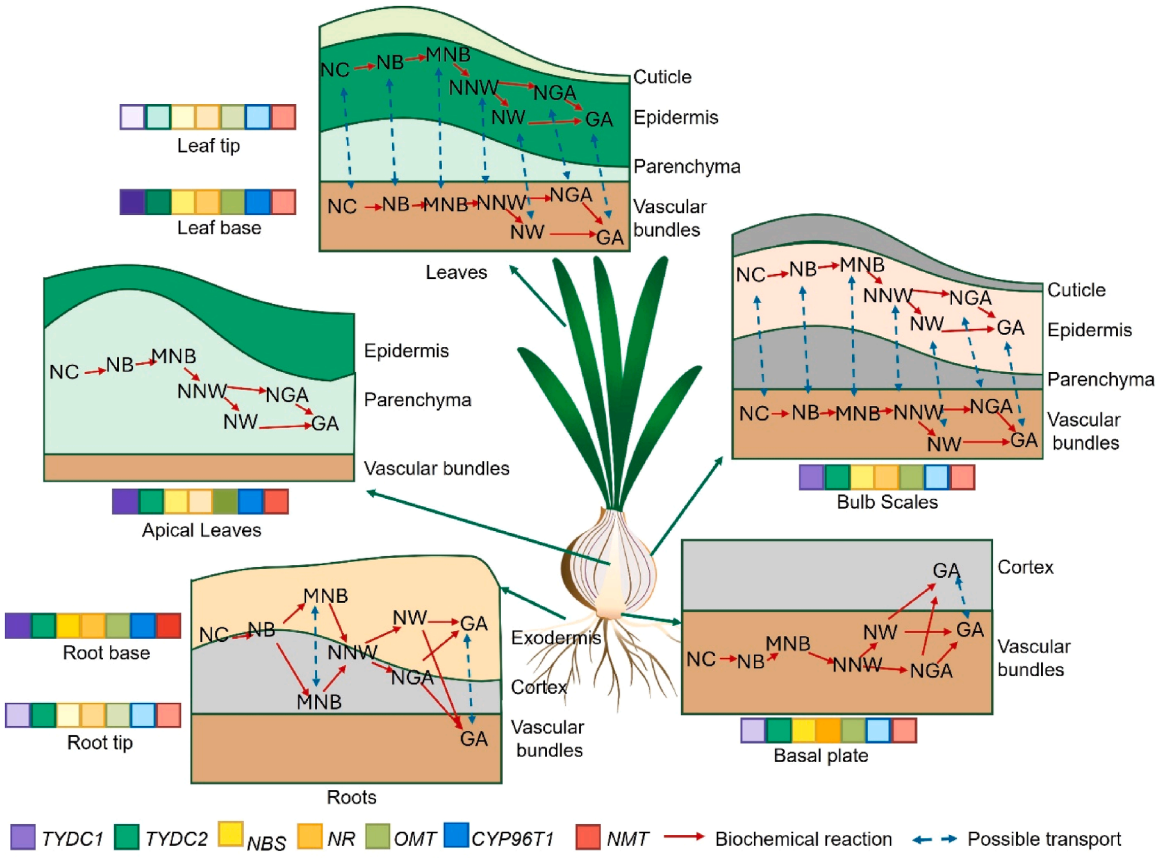

Fig. 9. The proposed biosynthetic pathway for galanthamine in *Hippeastrum papilio* is illustrated, with red arrows denoting biochemical steps and blue arrows indicating potential alkaloid transport. The pathway in the top is restricted to the leaves and the bulbs, and the bottom pathway belongs to the roots. The data presented in this study suggest that the early steps of AA biosynthesis are enriched in apical leaves, and that galanthamine biosynthesis likely occurs in distinct tissue-specific compartments, with varying degrees of metabolic exchange between these regions. In the leaves and bulbs, the pathway appears to be localized primarily in the epidermal tissues and vascular areas, while precursors were comparatively enriched in the apical leaves. The presence of key intermediates in both tissues indicates that biosynthetic reactions may occur in either compartment, with potential metabolite exchange between the epidermis and vascular areas. This suggests a dynamic interplay between these regions, in which specific steps of the pathway may be restricted to either the epidermis or the vascular tissues, followed by the transport of intermediates to the other compartment for subsequent reactions. In contrast, the roots exhibit a more compartmentalized biosynthetic profile. The limited exchange of intermediates observed in the roots, compared to the leaves and bulbs, implies that the reactions may be more spatially restricted. This compartmentalization could reflect a specialized metabolic strategy in the roots, potentially optimizing resource use or minimizing exposure of toxic intermediates to other tissues.

the middle bulb scales. Intriguingly, while most intermediates were detected in apical leaves, end-products AAs, except haemanthamine, were not. This suggested that the apical leaves could play an important role in early alkaloid biosynthesis in *H. papilio*. The higher abundance of galanthamine in outer bulb scales and basal plates, which are more exposed to the external environment, suggests a potential defensive role against herbivores or pathogens. Our results differ from those of Haist et al., which showed a high accumulation of all AAs, including galanthamine, in the inner bulb sections of *H. papilio*. However, this study used a less sensitive method [19]. The results did not align with the findings by Nakagawa et al. [43], who reported higher galanthamine levels in the apex leaves of *N. tazetta* bulbs [43]. Still, the basal plates were not examined in this study of a different Amaryllidaceae species. Compared to the subterranean bulbs of *N. tazetta, H. papilio* is an epiphyte, and its bulb is more exposed, which may necessitate different defense strategies. Alteration in withanolide levels in the aeroponically cultivated medicinal plant *Withania somnifera*, in which withanolides typically accumulate in the roots, initiates in the leaves as they develop aeroponically [53]. Thus, differences in growth conditions could also complicate the comparison of the biosynthesis of AA of *H. papilio* with geophytic species like *N. tazetta* or *Narcissus* cv. Tête-à-Tête [39].

Consistent with our analysis of the bulb, histochemical staining studies in *H. papilio* indicated that AAs were primarily localized in intercellular spaces, vacuoles, and nuclei, rather than in outer cell layers, such as the cuticle [19]. The abundance of alkaloids around vascular regions in the basal plates could suggest a potential role in nutrient transport or storage. While most alkaloids were more specific to the vascular bundles, galanthamine was present in both the parenchymal and vascular bundles of the basal plates. This reinforces the particular physiological function of this metabolite, while its ubiquity is consistent with its high abundance in the species.

4.3. Root tissues

A unique distribution pattern of alkaloids was observed in *H. papilio* root tissues, with more complex, compartmentalized features than in leaves and bulbs. One of the most intriguing observations was a specific intense accumulation of galanthamine, and to a lesser extent, of 4'-O-methylnorbelladine/norgalanthamine/normaritidine and 11β-hydroxygalanthamine in the vascular regions of the roots. This contrasted with leaves and bulbs, where vascular areas showed a high abundance of most alkaloids. Histochemical staining of *H. papilio* roots has previously shown that alkaloids are present in all three main regions—exodermis, cortex, and vascular cylinder —with higher intensity in the vascular area [19]. However, these findings represent the cumulative presence of all AAs, making it difficult to compare with the specific distribution

patterns of individual alkaloids observed in this study. Because epidermal and exodermal tissues are exposed to the environment, the chemical defense mechanism may be highly active in those areas. For example, it has been shown that defense-responsive genes are expressed in wheat epidermal cells in response to pathogen attack [1]. The compartmentalized distribution of AAs in root tissues suggests a highly regulated biosynthetic pathway, which may be tailored to the specific physiological and ecological roles of these compounds in *H. papilio*.

4.4. Differences in the precursors' distribution in H. papilio

Multivariate analysis in MSI studies often relies on quantitative ion intensities. Instead, we applied a hybrid matrix that integrates binary fine-localization patterns and the normalized frequency of organ-level detection. Recent advances in plant MSI analysis have increasingly highlighted the importance of such approaches for uncovering hidden biological organization [13,21,33,8], and our study extends these concepts to the investigation of specialized metabolite biosynthesis and transport in Amaryllidaceae.

This analysis revealed a clear spatial separation between precursor alkaloids (e.g., norbelladine, norcraugsodine, narwedine, nornarwedine/vittatine/noroxomaritidine) and downstream galanthamine-type and papiline-type compounds, with haemanthamine clustering with precursors. This observation suggests that early and late stages of the Amaryllidaceae alkaloid biosynthetic pathway may occur in spatially distinct tissues in *H. papilio*, consistent with the notion of tissue-specific partitioning of specialized metabolism. The clustering of precursors and intermediates was significantly associated with their enrichment in the apical bulb leaf, likely corresponding to the youngest and most biosynthetically active tissue. These results are partially consistent with Mehta et al.'s hypothesis that biosynthesis is more active in young tissues of leaves, even though they did not investigate young apical leaves [39]. However, these compounds were also frequently detected in the epidermis of the bulb mid-section and in the leaf base and mid-section, indicating that early biosynthetic steps may occur across both internal and peripheral tissues. This broader spatial distribution is in line with Haist et al., who reported high alkaloid concentrations in inner bulb tissues, but also observed signal in more superficial tissues, depending on compound type.

The consistent association of haemanthamine with precursors further suggests that this compound may be synthesized closer to the precursor zone than previously assumed. In contrast, galanthamine, 11β-hydroxygalanthamine, and papiline-type alkaloids clustered with features such as the root endodermis, leaf tip vascular bundles, and epidermal zones of distal organs, together with the detection of high levels of end-products in bulb and leaves mucilage, this suggests that late-stage tailoring may occur in more specialized cell layers, vascular-associated cells, distinct from the tissues synthesizing early intermediates. These spatial relationships reveal a likely progression from early, distributed biosynthesis to more compartmentalized localization of end products. Alternatively, active transport mechanisms could mediate the relocalization of galanthamine from its site of synthesis to specialized storage compartments, potentially minimizing self-toxicity or optimizing resource allocation within the plant. Consistently, Wang et al. previously showed that an ATP-binding cassette transporter (ABCB11) was involved in lycorine transport in *Lycoris aurea*. ABCB11 was detected in both leaves and bulbs, as well as the cortical cells of roots. Wang et al., [51]. The involvement of such transporter in *H. papilio* remains to be explored.

These clustering patterns should be interpreted as exploratory correlations rather than definitive biosynthetic maps, given the qualitative or semi-quantitative nature of the MSI analysis and the sampling that was performed during the vegetative stage. Another limitation of the current analysis was the presence of isomers (same *m/z*) for 4'-O-methylnorbelladine (norgalanthamine, normaritidine) and nornarwedine (vittatine/ noroxomaritidine), which introduced signal overlap in these cases.

Nonetheless, the consistent separation between precursor and galanthamine-type compounds across unsupervised clustering, PCA, and t-SNE, along with their reproducible association with distinct tissue features, provides a strong foundation for future work combining enzyme localization, gene expression, and transport assays to test these hypotheses experimentally.

At the transcript level, the qRT-PCR profiles reinforced our MSI-based interpretation of spatially organized alkaloid biosynthesis. While variability was observed in the distribution of *TYDC1/2* expression among root, stem, or leaf tissues using organ-level sampling methods in *Leucojum aestivum* and *Lycoris radiata* [23,27], here, we show that they were enriched more specifically in leaf bases of *H. papilio*. *NBS* was strongly expressed at the root base, mirroring findings in *Narcissus papyraceus* and *L. aestivum,* and supporting roots as possible sites of scaffold condensation and terminal tailoring converge [36]. In contrast, *OMT* and *CYP96T1* peaked in apical bulb leaves, consistent with proposals that young tissues are hotspots for phenol-coupling and diversification [39]. *NR* expression remained uniformly low, consistent with previous studies showing a poor correlation between *NR* transcript levels and alkaloid abundance [36]. Overall, the biosynthesis of AA in *H. papilio* did not exhibit a restrictive organ-specific pattern, with biosynthetic gene expression detected across all organs. Higher expression in specific organs could suggest a spatial division of biosynthetic steps: precursor supply in leaf bases, scaffold formation and late tailoring in basal/root zones, and coupling/diversification in apical leaves. A tissue-level separation echoes models from other alkaloid systems, such as *Papaver somniferum* and *Catharanthus roseus*. It underscores the coordinated, multi-organ nature of Amaryllidaceae alkaloid biosynthesis in *H. papilio* [52] (Fig. 9).

Further investigation, including multi-omics or single-cell-level analysis, is needed to elucidate the pathway and identify which cells are responsible for each biosynthetic step. Likewise, isotopic labelling experiments would clarify the extent of metabolite transport versus local synthesis, distinguishing true biosynthetic sites from accumulation zones. Such integrative strategies will be essential to fully resolve the cellular and organ-level biosynthetic map of Amaryllidaceae alkaloids.

Although our data suggest a broader biosynthetic landscape than previously documented, biosynthetic models may differ across Amaryllidaceae species. MS imaging captures steady-state distributions rather than flux, and differences between *H. papilio* and other genera (e.g., *Narcissus*, *Lycoris*, *Leucojum*) underscore the importance of species-specific analyses.

4.5. New metabolites uncovered in H. papilio

By leveraging multiple databases integrated with Metaspace, we identified several previously unreported AAs in *H. papilio*, expanding the known phytochemical profile of this species. Notably, our findings also provide evidence for compounds associated with colchicine biosynthesis, a pathway previously documented only in *Lycoris radiata* [54]. The detection of multiple intermediates in this pathway supports the possibility of shared or convergent biosynthetic routes within the Amaryllidaceae family. Additionally, we observed diverse alkaloid groups beyond the typical Amaryllidaceae-type structures, underscoring the metabolic complexity of this plant family [25,5]. Beyond targeted alkaloid profiling, this non-targeted approach proves valuable for broader metabolomic investigations. The simultaneous detection of flavonoids, lignans, pigments, and other specialized metabolites highlights the potential of MALDI-MS in studying metabolic correlations, plant-environment interactions, and biosynthetic networks. Such comprehensive analyses could pave the way for future research on the ecological and physiological roles of diverse metabolite classes in plants.

5. Conclusion

To the best of our knowledge, this is the first comprehensive study of the spatial metabolic arrangement of alkaloids in an Amaryllidaceae species. Our analysis revealed that galanthamine-type and papiline-type AAs exhibited a consistent spatial arrangement in the organs of *H. papilio,* which differed from that of intermediates and haemanthamine. The abundance of AAs in epidermal and vascular tissues highlights their potential role in defense mechanisms, while the presence of biosynthetic intermediates suggests widespread alkaloid biosynthesis. In leaves, the spatial distribution of metabolites appears interdependent: areas with early intermediates consistently show downstream metabolites, and, conversely, regions with lower precursor detection show reduced AA detection. In bulbs, while intermediates and end-products were detected in older scales and basal plates, intermediates were more specific to the apical leaves. In the basal plates, most localized in vascular bundles, while galanthamine was also abundant in the parenchyma. In roots, AAs were less prevalent in the vascular bundles than in the cortex, with galanthamine and its derivative being a notable exception. This unique accumulation pattern of galanthamine potentially indicates distinct transport or storage mechanisms compared to those of other alkaloids. These findings provide crucial insights into the tissue-specific biosynthesis and localization of AAs, emphasizing the coordinated nature of their production and storage across various plant organs. This work provides the first multi-organ MALDI-MSI atlas for a high-galanthamine-producing *Hippeastrum* species, offering a compound-resolved spatial perspective that complements and extends previous studies in other Amaryllidaceae genera. By revealing that both intermediates and end-products are present across diverse tissues, our findings lay a foundation for understanding the coordinated biosynthesis of AAs in *H. papilio* and highlight the species' potential for biotechnological alkaloid production.

CRediT authorship contribution statement

Nuwan Sameera Liyanage: Conceptualization, Methodology, Experiments, Analysis, Writing- Original draft, Writing- Reviewing and Editing; **Natacha Merindol:** Analysis, supervision**,** Writing- Reviewing and Editing; **Sajjad Sobhanverdi**: qRT-PCR Experiments, Writing- Reviewing and Editing **Kenneth Munk Pedersen:** LC-MS and analysis, Writing- Reviewing and Editing; **Christian Janfelt:** Conceptualization, Methodology, Resources, supervision, funding acquisition, Writing- Original draft, Writing- Reviewing and Editing **Isabel Desgagné-Penix:** Conceptualization, Resources, supervision, funding acquisition, Writing- Original draft, Writing- Reviewing and Editing.

Funding

This research was funded by Canada Research Chair on plant specialized metabolism Award No CRC-2018–00137 to IDP. Thanks are extended to the Canadian taxpayers and to the Canadian government for supporting the Canada Research Chairs Program. Additional support from the Natural Sciences and Engineering Research Council of Canada (NSERC) award number RGPIN/3218–2021 to IDP. Funding from the Carlsberg Foundation and Independent Research Fund Denmark | Medical Sciences (grant no. DFF – 4002–00391) for MALDI-MSI instrumentation to CJ is gratefully acknowledged.

Declaration of Competing Interest

The authors declare the following financial interests/personal relationships which may be considered as potential competing interests: Isabel Desgagne-Penix reports financial support was provided by Canada Research Chairs Program. Isabel Desgagne-Penix reports financial support was provided by Natural Sciences and Engineering Research Council of Canada. Christian Janfelt reports financial support was provided by Carlsberg Foundation. If there are other authors, they declare that they have no known competing financial interests or personal relationships that could have appeared to influence the work reported in this paper.

Acknowledgements

The authors thank Dr. Marcus Daniel Brandbjerg Bohn Lorensen (University of Copenhagen), Dr Karen Cristine Gonçalves Dos Santos, and Rohith Grandhi (Université du Québec à Trois-Rivières) for their valuable input and contributions. We also thank Prof. Antonio Evidente (Universitario Monte Sant'Angelo, Naples, Italy) for providing some alkaloid standards. During the preparation of this work, the authors used ChatGPT version 4.0, a free AI language model, in order to write the scripts in Python, correct grammatical errors and enhance readability. After using this tool, the authors reviewed and edited the content as needed and take full responsibility for the content of the publication.

Appendix A. Supporting information

Supplementary data associated with this article can be found in the online version at doi:10.1016/j.cpb.2026.100579.

Data availability

Data will be made available on request.

References

[1] Fredy Altpeter, Alok Varshney, Olaf Abderhalden, Dimitar Douchkov, Christof Sautter, Jochen Kumlehn, Robert Dudler, Patrick Schweizer, Stable expression of a defense-related gene in wheat epidermis under transcriptional control of a novel promoter confers pathogen resistance, Plant Mol. Biol. 57 (2005) 271–283.
[2] de Andrade, Jean Paulo, Strahil Berkov, Francesc Viladomat, Carles Codina, José Angelo S Zuanazzi, Jaume Bastida, Alkaloids from Hippeastrum papilio, Molecules 16 (2011) 7097–7104.
[3] Lamichhane Basanta, Sarah-Eve Gélinas, Natacha Merindol, Manoj Koirala, Karen Cristine Gonçalves Dos Santos, Hugo Germain, Isabel Desgagné-Penix, Elucidating the enzyme network driving Amaryllidaceae alkaloids biosynthesis in Leucojum aestivum, Plant Biotechnol. J. (2025).
[4] Strahil Berkov, Lilyia Georgieva, Boriana Sidjimova, Jaume Bastida, Evaluation of Hippeastrum papilio (Ravenna) Van Scheepen potencial as a new industrial source of galanthamine, Ind. Crops Prod. 178 (2022) 114619.
[5] Strahil Berkov, Edison Osorio, Francesc Viladomat, Jaume Bastida, Chemodiversity, chemotaxonomy and chemoecology of Amaryllidaceae alkaloids, Alkaloid. Chem. Biol. 83 (2020) 113–185.
[6] Nanna Bjarnholt, Bin Li, Janina D'Alvise, Christian Janfelt, Mass spectrometry imaging of plant metabolites–principles and possibilities, Nat. Prod. Rep. 31 (2014) 818–837.
[7] Bokhart, Mark T, Milad Nazari, Kenneth P. Garrard, David C. Muddiman, 'MSiReader v1. 0: evolving open-source mass spectrometry imaging software for targeted and untargeted analyses', J. Am. Soc. Mass Spectrom. 29 (8-16) (2017).
[8] B.A. Boughton, D. Thinagaran, D. Sarabia, A. Bacic, U. Roessner, Mass spectrometry imaging for plant biology: a review, Phytochem Rev. 15 (2016) 445–488.
[9] Antonio Campos-Rocha, Meerow Alan William, Peixoto Mauro, Ingrid Koch, Patrícia Aparecida Messias, Antoinette Dutilh Julie Henriette, To print in red ink, Plant Ecol. Evol. 156 (2023) 239–256.
[10] Marie Chavent, Kuentz-Simonet Vanessa, Liquet Benoît, Saracco Jérôme, ClustOfVar: an R package for the clustering of variables, J. Stat. Softw. 50 (2012) 1–16.
[11] Karl-Josef Dietz, Wolfram Hartung, The leaf epidermis: its ecophysiological significance. Progress in Botany/Fortschritte der Botanik: Structural Botany Physiology Genetics Taxonomy Geobotany/Struktur Physiologie Genetik Systematik Geobotanik, Springer, 1996.
[12] Lloyd Donaldson, Autofluorescence in plants, Molecules 25 (2020) 2393.
[13] Yonghui Dong, Li Bin, Malitsky Sergey, Rogachev Ilana, Aharoni Asaph, Kaftan Filip, Svatoš. Aleš, Franceschi Pietro, 'Sample preparation for mass spectrometry imaging of plant tissues: a review', Front. Plant Sci. 7 (2016) 60.
[14] Govaerts, R. 'Subgenera: H. subg. Hippeastrum–H. subg. Tocantinia'.
[15] Granborg, Jonatan Riber, Anne Mette Handler, Christian Janfelt, 'Mass spectrometry imaging in drug distribution and drug metabolism studies–principles, applications and perspectives', TrAC Trends Anal. Chem. 146 (2022) 116482.
[16] Ying Guo, de Andrade Jean P, B.Pigni Natalia, Torras-Claveria Laura, R. Tallini Luciana, S.Borges Warley de, Francesc Viladomat, Jerald J Nair, José A.

S. Zuanazzi, Jaume Bastida, 'New alkaloids from Hippeastrum papilio (Ravenna) van Scheepen', Helv. Chim. Acta 99 (2016) 143–147.
[17] Habib, M. Abdel-Azim, False-positive alkaloid reactions, J. Pharm. Sci. 69 (1980) 37–43.
[18] Hagel, Jillian M, Akpevwe Onoyovwi, Edward C. Yeung, Peter J. Facchini, Role of phloem metabolites in plant defense. Phloem: Molecular Cell Biology, Systemic Communication, Biotic Interactions, 2012, pp. 249–270.
[19] Gabriela Haist, Boriana Sidjimova, Elina Yankova-Tsvetkova, Milena Nikolova, Rumen Denev, Ivanka Semerdjieva, Jaume Bastida, Strahil Berkov, Metabolite profiling and histochemical localization of alkaloids in Hippeastrum papilio (Ravena) van Scheepen, J. Plant Physiol. (2024) 154223.
[20] Heinrich, Michael, Hooi Lee Teoh, Galanthamine from snowdrop—the development of a modern drug against Alzheimer's disease from local Caucasian knowledge, J. Ethnopharmacol. 92 (2004) 147–162.
[21] Heyman, M. Heino, Ian A. Dubery, The potential of mass spectrometry imaging in plant metabolomics: a review, Phytochem. Rev. 15 (2016) 297–316.
[22] Patrick J. Horn, Kent D. Chapman, Imaging plant metabolism in situ, J. Exp. Bot. 75 (2024) 1654–1670.
[23] Jiawei Hu, Wei Li, Zhan Liu, Guolin Zhang, Yinggang Luo, Molecular cloning and functional characterization of tyrosine decarboxylases from galanthamine-producing Lycoris radiata, Acta Physiol. Plant. 43 (2021) 84.
[24] Thilina U. Jayawardena, Natacha Merindol, Nuwan Sameera Liyanage, Isabel Desgagné-Penix, Unveiling Amaryllidaceae alkaloids: from biosynthesis to antiviral potential–a review, Nat. Prod. Rep. (2024).
[25] Zhong Jin, Guangmin Yao, Amaryllidaceae and Sceletium alkaloids, Nat. Prod. Rep. 36 (2019) 1462–1488.
[26] Seydou Ka, Manoj Koirala, Natacha Mérindol, Isabel Desgagné-Penix, Biosynthesis and biological activities of newly discovered Amaryllidaceae alkaloids, Molecules 25 (2020) 4901.
[27] V. Karimzadegan, M. Koirala, S. Sobhanverdi, N. Merindol, B.B. Majhi, S. Gélinas, V.I. Timokhin, J. Ralph, M. Dastmalchi, I. Desgagné-Penix, Characterization of cinnamate 4-hydroxylase (CYP73A) and p-coumaroyl 3′-hydroxylase (CYP98A) from Leucojum aestivum, a source of Amaryllidaceae alkaloids, Plant Physiol. Biochem. 210 (2024) 108612.
[28] Leonard Kaufman, J.Rousseeuw Peter, Finding groups in data: an introduction to cluster analysis, John Wiley & Sons, 2009.
[29] Tadafumi Kawamoto, Use of a new adhesive film for the preparation of multi-purpose fresh-frozen sections from hard tissues, whole-animals, insects and plants, Arch. Histol. Cytol. 66 (2003) 123–143.
[30] Tadafumi Kawamoto, Komei Kawamoto, Preparation of thin frozen sections from nonfixed and undecalcified hard tissues using Kawamoto's film method (2020). Skeletal development repair Methods protocols, 2021, pp. 259–281.
[31] Kilgore, Matthew B, Megan M. Augustin, Gregory D. May, John A. Crow, Toni M. Kutchan, CYP96T1 of Narcissus sp. aff. Pseudonarcissus catalyzes formation of the Para-Para'CC phenol couple in the Amaryllidaceae alkaloids, Front. Plant Sci. 7 (2016) 225.
[32] B. Lamichhane, S.E. Gelinas, N. Merindol, M. Koirala, K.C.G. Dos Santos, H. Germain, I. Desgagne-Penix, Elucidating the enzyme network driving Amaryllidaceae alkaloids biosynthesis in Leucojum aestivum, Plant Biotechnol. J. (2025).
[33] Ying Li, Erich Grotewold, Natalia Dudareva, Enough is enough: feedback control of specialized metabolism, Trends Plant Sci. 29 (2024) 514–523.
[34] Liyanage, Nuwan Sameera, Basanta Lamichhane, Elisa Fantino, Natacha Mérindol, Sarah-Eve Gélinas, Maria Camila García Tobón, Isabel Desgagné-Penix, Coclaurine N-methyltransferase-like enzymes drive the final biosynthetic reaction of the anti-Alzheimer's drug galanthamine in Amaryllidaceae, Plant Physiol. Biochem. (2025) 110067.
[35] Clement Loy, Lon Schneider, Galantamine for Alzheimer's disease and mild cognitive impairment, Cochrane Database Syst. Rev. (2006).
[36] Bharat Bhusan Majhi, Sarah-Eve Gélinas, Natacha Mérindol, Simon Ricard, Isabel Desgagné-Penix, Characterization of norbelladine synthase and noroxomaritidine/norcraugsodine reductase reveals a novel catalytic route for the biosynthesis of Amaryllidaceae alkaloids including the Alzheimer's drug galanthamine, Front. Plant Sci. 14 (2023).
[37] Alan W. Meerow, Elliot M. Gardner, Kyoko Nakamura, Phylogenomics of the Andean tetraploid clade of the American Amaryllidaceae (subfamily Amaryllidoideae): unlocking a polyploid generic radiation abetted by continental geodynamics, Front. Plant Sci. 11 (2020) 582422.
[38] A.W. Meerow, D.A. Snijman, Amaryllidaceae. Flowering Plants· Monocotyledons: Lilianae (except Orchidaceae), Springer, 1998.
[39] Niraj Mehta, Yifan Meng, Richard Zare, Rina Kamenetsky-Goldstein, Elizabeth Sattely, A developmental gradient reveals biosynthetic pathways to eukaryotic toxins in monocot geophytes, Cell 187 (5620-37) (2024) e10.
[40] L. Meisel, B. Fonseca, S. Gonzalez, R. Baeza-Yates, V. Cambiazo, R. Campos, M. Gonzalez, A. Orellana, J. Retamales, H. Silva, A rapid and efficient method for purifying high quality total RNA from peaches (*Prunus persica*) for functional genomics analyses, Biol. Res 38 (2005) 83–88.
[41] Lucia Montini, Christoph Crocoll, Roslyn M. Gleadow, Mohammed Saddik Motawia, Christian Janfelt, Nanna Bjarnholt, Matrix-assisted laser desorption/ionization-mass spectrometry imaging of metabolites during sorghum germination, Plant Physiol. 183 (2020) 925–942.
[42] Jerald J. Nair, Johannes van Staden, Pharmacological and toxicological insights to the South African Amaryllidaceae, Food Chem. Toxicol. 62 (2013) 262–275.
[43] Kaoru Nakagawa, Tetsuo Iida, Manami Kobayashi, Shuichi Shimma, Combination of probe electrospray ionization mass spectrometry and mass spectrometry imaging to analyze plant alkaloids in narcissus tazetta, Mass Spectrom. 13 (2024). A0163-A0163.
[44] Andrew Palmer, Prasad Phapale, Ilya Chernyavsky, Regis Lavigne, Dominik Fay, Artem Tarasov, Vitaly Kovalev, Jens Fuchser, Sergey Nikolenko, Charles Pineau, FDR-controlled metabolite annotation for high-resolution imaging mass spectrometry, Nat. Methods 14 (2017) 57–60.
[45] Liang Qin, Yawen Zhang, Yaqin Liu, Huixin He, Manman Han, Yanyan Li, Maomao Zeng, Xiaodong Wang, Recent advances in matrix-assisted laser desorption/ionisation mass spectrometry imaging (MALDI-MSI) for in situ analysis of endogenous molecules in plants, Phytochem. Anal. 29 (2018) 351–364.
[46] Thorsten Schramm, Zoë Hester, Ivo Klinkert, Jean-Pierre Both, Ron M.A. Heeren, Alain Brunelle, Olivier Laprévote, Nicolas Desbenoit, Marie-France Robbe, Markus Stoeckli, imzML—a common data format for the flexible exchange and processing of mass spectrometry imaging data, J. Proteom. 75 (2012) 5106–5110.
[47] Bernhard Spengler, Mass spectrometry imaging of biomolecular information, Anal. Chem. 87 (2015) 64–82.
[48] Markus Stoeckli, Dieter Staab, Michael Wetzel, Matthias Brechbuehl, iMatrixSpray: a free and open source sample preparation device for mass spectrometric imaging, Chimia 68 (2014), 146-146.
[49] Tallini, Luciana R, Raquel B. Giordani, Jean Paulo de Andrade, Jaume Bastida, José Angelo S. Zuanazzi, Structural diversity and biological potential of alkaloids from the genus Hippeastrum, Amaryllidaceae: an update, Rev. Bras. De. Farmacogn. 31 (2021) 648–657.
[50] Alain Tissier, Jörg Ziegler, Thomas Vogt, Specialized plant metabolites: diversity and biosynthesis. Ecological biochemistry environmental interspecies interactions, 2014, pp. 14–37.
[51] R. Wang, Y. Liu, S. Xu, J. Li, J. Zhou, R. Wang, An ATP-binding cassette transporter, LaABCB11, contributes to alkaloid transport in Lycoris aurea, Int J. Mol. Sci. 22 (2021).
[52] Jacinta L. Watkins, Peter J. Facchini, Compartmentalization at the interface of primary and alkaloid metabolism, Curr. Opin. Plant Biol. 66 (2022) 102186.
[53] Ya-ming Xu, Song Gao, Daniel P. Bunting, A.A. Leslie Gunatilaka, Unusual withanolides from aeroponically grown Withania somnifera, Phytochemistry 72 (6) (2011) 518–522.
[54] He Yan, Na Xie, Chenquan Zhong, Anqi Su, Xiaoli Hui, Xin Zhang, Zhao Jin, Zhipeng Li, Juntao Feng, Jun He, Aphicidal activities of Amaryllidaceae alkaloids from bulbs of Lycoris radiata against Aphis citricola, Ind. Crops Prod. 123 (2018) 372–378.